JCS ePress online publication date 27 January 2009

Drebrin A regulates dendritic spine plasticity and synaptic function in mature cultured hippocampal neurons

Anton Ivanov[1], Monique Esclapez[2], Christophe Pellegrino[1], Tomoaki Shirao[3] and Lotfi Ferhat[1,4,*]

[1]INMED/INSERM U29, Parc Scientifique de Luminy, 13273, Marseille, France
[2]INSERM U 751, Université d'Aix-Marseille, Hôpital de la Timone, Marseille, France
[3]Department of Neurobiology and Behavior, Gunma University Graduate School of Medicine, Maebashi, Gunma, Japan
[4]CNRS UMR 6184, Neurobiologie des Interactions Cellulaires et Neurophysiopathologie (NICN), IFR Jean Roche, Marseille, F-13020, France
*Author for correspondence (e-mail: lotfi.ferhat@univmed.fr)

Accepted 30 October 2008
Journal of Cell Science 122, 524-534 Published by The Company of Biologists 2009
doi:10.1242/jcs.033464

Summary

Drebrin A, one of the most abundant neuron-specific F-actin-binding proteins, is found exclusively in dendrites and is particularly concentrated in dendritic spines receiving excitatory inputs. We investigated the role of drebrin A in synaptic transmission and found that overexpression of drebrin A augmented the glutamatergic synaptic transmission, probably through an increase of active synaptic site density. Interestingly, overexpression of drebrin A also affected the frequency, amplitude and kinetics of miniature inhibitory postsynaptic currents (mIPSCs), despite the fact that GABAergic synapse density and transmission efficacy were not modified. Downregulation of drebrin A led to a decrease of both glutamatergic and GABAergic synaptic activity. In heterologous cells, drebrin A reorganized and stabilized F-actin and these effects were mediated by its actin-binding domain. Thus, drebrin A might regulate dendritic spine morphology via regulation of actin cytoskeleton remodeling and dynamics. Our data demonstrate for the first time that drebrin A modulates glutamatergic and GABAergic synaptic activities.

Supplementary material available online at
http://jcs.biologists.org/cgi/content/full/122/4/524/DC1

Key words: Spine morphogenesis, F-actin, GABA, Glutamate, vGlut1, Gad-65, Bassoon

Introduction

Dendritic spines are the postsynaptic elements that receive the majority of excitatory glutamatergic inputs in the CNS (Harris and Kater, 1994). These small protrusions emerging from dendritic shafts are believed to constitute sites for the development of glutamatergic neuronal networks and might be a cellular substrate for synaptic plasticity (Yuste and Bonhoeffer, 2001).

The actin filament (F-actin) is one of the major structural elements of dendritic spines (Fifkova and Delay, 1982; Matus et al., 1982). These actin filaments are thought to be the key target of molecular mechanisms regulating spine plasticity that has been shown to be activity dependent (Matus, 2000). The adult isoform of drebrin, drebrin A (DA), a major neuron-specific F-actin-binding protein, emerges as a candidate protein that regulates the actin cytoskeleton of dendritic spines (Sekino et al., 2007). DA is specifically localized at dendritic spines of mature cortical neurons (Hayashi et al., 1996; Aoki et al., 2005) and is known to inhibit the actin-binding activity of tropomyosin, fascin and α-actinin (Ishikawa et al., 1994; Sasaki et al., 1996). In vitro, it also inhibits the interaction between actin and myosin (Hayashi et al., 1996; Ishikawa et al., 2007), suggesting that it modulates actin filament contractility. Transfection of DA into fibroblasts induced reorganization of actin filaments, leading to a change in cell morphology (Shirao et al., 1994). Such transfection in neurons results in the elongation of dendritic spines of cortical neurons (Hayashi and Shirao, 1999). Furthermore, downregulation of DA expression in developing hippocampal neurons suppresses the accumulation of F-actin within dendritic spines (Takahashi et al., 2003).

In addition to its role in spine morphology, DA might be involved in spine functions. It has been recently shown that DA is involved in spinous clustering of the postsynaptic density (PSD) scaffold protein, PSD-95 (Takahashi et al., 2003), as well as in the activity-dependent synaptic targeting of N-methyl-D-aspartate (NMDA) subtype of glutamate receptors (Takahashi et al., 2006). Consistent with this observation, the induction of long-term potentiation (LTP) in the hippocampus is accompanied by the enhanced DA content within dendritic spines (Fukazawa et al., 2003). All these data support the hypothesis that DA expressed in spines can modulate synaptic activity.

To test this hypothesis, we investigated the effects of DA on dendritic spine morphology and its consequences on synaptic activity, in mature cultured hippocampal neurons. Our study led to three main conclusions: (1) the actin-binding domain of DA is responsible for dendritic spine plasticity, presumably via regulation of actin cytoskeleton remodeling and dynamics; (2) enhanced expression of DA increases the density of glutamatergic but not GABAergic synapses and leads to alteration of the normal excitatory-inhibitory balance in favour of excitation; (3) downregulation of DA results in the decrease of both glutamatergic and GABAergic synaptic transmissions without affecting the normal excitatory-inhibitory balance. Thus, the present study provides the first evidence that an actin-binding protein such as DA modulates both glutamatergic and GABAergic synaptic transmission in mature hippocampal neurons.

Results

Postsynaptic localization of endogenous DA in mixed hippocampal cultures

The developmental changes of DA localization in hippocampal neurons have been described in low-density culture from 7 to 21 days in vitro (DIV) (Takahashi et al., 2003). In this study, we re-examined this issue in mixed high-density hippocampal cultures (supplementary material Fig. S1A,B). Our data confirmed the postsynaptic localization of DA in mixed hippocampal neurons at 21 DIV, because it colocalized with two specific markers for the postsynaptic compartment, PSD-95 and F-actin, in most spines (supplementary material Fig. S1C-E).

The actin-binding domain of DA is responsible for spine morphological changes induced by overexpression of DA-GFP in mature hippocampal neurons

It has been shown that DA affects some morphological aspects of cortical dendritic spines (Hayashi and Shirao, 1999). To analyze the physiological consequences of morphological changes induced by DA, we re-examined the effects of DA on spine morphology in our mature and high-density hippocampal culture system. As revealed by cotransfected red fluorescent protein (RFP) neurons (Fig. 1A,B), both green fluorescent protein (GFP, used as a control) (Fig. 1A′) and DA-GFP (Fig. 1B′) were distributed within dendritic shafts, as well as in dendritic protrusions. With respect to DA-GFP, the green fluorescence in dendritic shafts was lighter than in dendritic protrusions. Striking morphological changes were observed between dendritic protrusions of DA-GFP- (Fig. 1B′) and those of GFP neurons (Fig. 1A′). Indeed, the dendrites of DA-GFP neurons displayed longer protrusions (Fig. 1B-B″, arrows) compared with those found in GFP neurons (Fig. 1A-A″). Some of these long protrusions reached over 5 μm (see asterisks in Fig. 1B-B″). All protrusions induced by DA-GFP included heads, and thus differed in their morphology from dendritic filopodia, which have no heads. These observations suggested that these long protrusions were spines and were more mature than filopodia, which are precursors of dendritic spines (Papa et al., 1995).

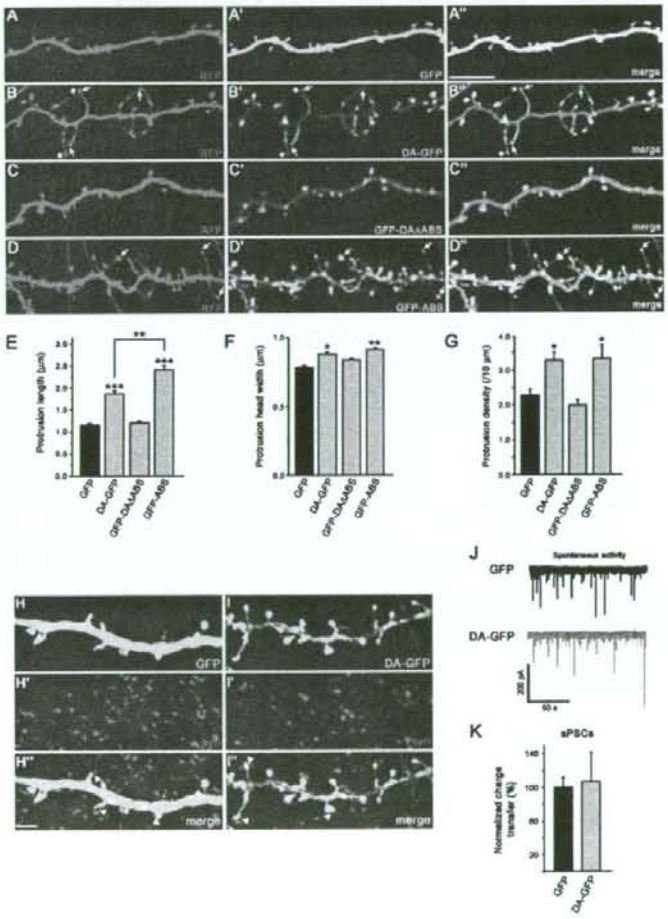

Fig. 1. Effects of DA-GFP overexpression on spine morphology and network activity. Cultured neurons were cotransfected on DIV 21 with RFP (A) and GFP (A′), RFP (B) and DA-GFP (B′), RFP (C) and GFP-DAΔABS (C′), or RFP (D) and GFP-ABS (D′). At 23 DIV, neurons were fixed and then analyzed. RFP channel is shown in all panels to outline dendritic morphology. (A″,B″,C″ and D″) Merged images. Scale bar: 10 μm. (E-G) Quantification of DA-GFP effects on protrusion plasticity. Histograms showing the average length (E), width (F) and density (G) of protrusions of GFP, DA-GFP, GFP-DAΔABS and GFP-ABS neurons. As with GFP spines (H-H″), the long spines induced by DA-GFP (I-I″) were associated with functional excitatory synaptic contacts. GFP (H) or DA-GFP (I) neurons immunostained for synaptophysin (H′ and I′). (H″ and I″) Merged images. Some synaptophysin clusters are not in close apposition to the spines of GFP or DA-GFP neurons because they are probably opposed to dendritic shafts or spines of nontransfected neurons. Scale bar: 10 μm. *P<0.05, **P<0.01, ***P<0.001, Bonferroni's test. (J) Examples of sPSCs recorded at –60 mV in GFP (black trace) and DA-GFP neurons (gray trace). (K) Histogram showing the sPSCs charge transfer in all recorded GFP and DA-GFP neurons. All data in E-G and K are mean ± s.e.m.

To investigate whether DA-GFP exerts its effects via its interaction with F-actin, we cotransfected mature hippocampal neurons with RFP (Fig. 1C) and GFP-DAΔABS (Fig. 1C′), a mutant of DA that lacks the actin-binding domain (Hayashi et al., 1999). As revealed by coexpressed RFP (Fig. 1C), GFP-DAΔABS (Fig. 1C′) was detected in dendritic shafts as well as at dendritic protrusions (Fig. 1C″). In contrast to DA-GFP, GFP-DAΔABS did not induce elongation of dendritic protrusions (Fig. 1C-C″). These data indicate that the elongation of dendritic protrusions induced by DA-GFP requires its actin-binding domain.

We further determined whether the overexpression of the actin-binding domain of DA was sufficient to induce the elongation of dendritic protrusions. For this purpose, we cotransfected hippocampal neurons with RFP (Fig. 1D) and GFP-ABS (Fig. 1D′), a construct that contains only the actin-binding domain of DA (Hayashi et al., 1999). As visualized by cotransfected RFP (Fig. 1D), GFP-ABS was found in dendritic shafts as well as in dendritic protrusions (Fig. 1D″). Similarly to DA-GFP, GFP-ABS induced morphological changes in dendritic protrusions. Indeed, some dendritic protrusions of GFP-ABS neurons were markedly longer (Fig. 1D-D″, see arrows) than those observed in GFP neurons (Fig. 1A-A″). In addition, GFP-ABS neurons displayed long protrusions with heads, reminiscent of dendritic spines. Therefore, the actin-binding domain of DA is necessary and sufficient to induce an effect on dendritic spine elongation.

Quantitative analysis in both DA-GFP and GFP-ABS neurons showed that the average protrusion lengths were significantly longer (1.86±0.08 and 2.40±0.10 μm, respectively) than that in GFP (1.15±0.04 μm; n=10; P<0.001; Bonferroni's test) (Fig. 1E) and GFP-DAΔABS neurons (1.15±0.04 and 1.21±0.04 μm, respectively; n=10; P<0.001; Bonferroni's test) (Fig. 1E). However, the average protrusion length of GFP-DAΔABS neurons was not significantly different from that of GFP neurons (P=0.38; Bonferroni's test) (Fig. 1E). Interestingly, the average protrusion of GFP-ABS was significantly longer than that in DA-GFP neurons (P<0.01; Bonferroni's test) (Fig. 1E), presumably due to their differences in expression levels. Indeed, western blot analyses on CHO-K1 cells showed higher expression levels of GFP-ABS compared with those of DA-GFP construct (data not shown).

In DA-GFP and GFP-ABS neurons, the average protrusion head width was significantly larger (0.88±0.02 and 0.91±0.01 μm, respectively) than that in GFP neurons (0.78±0.02 μm; n=10; P<0.05 for DA-GFP and P<0.01 for GFP-ABS; Bonferroni's test) (Fig. 1F). However, in GFP-DAΔABS neurons, the average protrusion head width (0.83±0.01 μm) was not different from that of GFP neurons (n=10; P=0.18; Bonferroni's test) (Fig. 1F).

In DA-GFP and GFP-ABS neurons, the average protrusion densities were significantly higher (3.28±0.23 and 3.32±0.39 spines/10 μm, respectively) than that in GFP neurons (2.29±0.17 spines/10 μm; n=10; P<0.05; Bonferroni's test) (Fig. 1G), whereas the average protrusion density of GFP-DAΔABS neurons (2.00±0.15 spines/10 μm) was not significantly different from that of GFP neurons (n=10; P=0.26; Bonferroni's test) (Fig. 1G). Therefore the actin-binding domain of DA was necessary and sufficient to induce an effect on spine morphology.

The molecular mechanisms by which DA-GFP causes elongation of dendritic spines was investigated. For this purpose, we overexpressed either DA-GFP or its DA mutants (GFP-DAΔABS and GFP-ABS) in CHO-K1 cells and analyzed its effects on the organization and stabilization of F-actin (supplementary material Figs S2 and S3, respectively). CHO-K1 cells were used because, in contrast to neurons, they provide a model of choice for visualizing the cellular organization and stability of F-actin (Rami et al., 2006). Studies in heterologous cells revealed that DA reorganized F-actin and stabilized them and these effects were dependent upon its actin-binding domain (supplementary material Figs S2 and S3, respectively).

Effects of DA-GFP overexpression on synaptic function

Our confocal microscopy data revealed that as for spines labeled with GFP (Fig. 1H-H″, see arrowheads), the long protrusions induced by DA-GFP (Fig. 1I) were associated with axon terminals since a presynaptic marker such as synaptophysin (Fig. 1I′) was facing most of these dendritic protrusions (Fig. 1I″, arrowheads). The close apposition of the presynaptic marker to the long spines induced by overexpression of DA-GFP suggests the presence of synaptic excitatory contacts. We next investigated whether these synapses were functional. Whole-cell recordings of spontaneous and miniature synaptic currents were performed on mature cultured hippocampal neurons overexpressing either GFP (used as a control, supplementary material Fig. S4) or DA-GFP. Our data showed that spontaneous activity was detected both in GFP or DA-GFP neurons (Fig. 1J), indicating that these neurons were alive and integrated in the neuronal network. In addition, the neuronal network activity was not affected by the overexpression of DA-GFP compared with that of GFP neurons. Indeed, the average charge transfer of spontaneous postsynaptic currents (sPSCs) was not significantly different in both culture types (GFP, 100±11%; DA-GFP, 106±35%; $n \geqslant 5$; P=0.8; U-test) (Fig. 1K).

Next, we investigated whether overexpression of DA-GFP was also associated with changes in the electrophysiological properties of excitatory glutamatergic synapses (Fig. 2A). In DA-GFP neurons, the cumulative probability plots of amplitude (Fig. 2B) and frequency (Fig. 2C) of miniature excitatory postsynaptic currents (mEPSCs) were significantly shifted to higher values compared with those of GFP neurons (n=8; P<0.01 for the amplitude and P<0.05 for the frequency; K-S test). The average amplitude and frequency of mEPSCs were increased in DA-GFP neurons (14.0±0.6 pA; 3.7±0.5 Hz) when compared with those of GFP neurons (11.8±0.4 pA, Fig. 2B, inset; 2.9±0.5 Hz, Fig. 2C, inset). However, the average rise times (GFP: 1.28±0.26 mseconds; DA-GFP: 1.16±0.11 mseconds; n=8; P=0.67; Student's t-test) (Fig. 2D) and decay times (GFP, 6.04±0.90 mseconds; DA-GFP, 6.39±0.79 mseconds; n=8; P=0.14; Student's t-test) (Fig. 2E) were comparable. As a result of the amplitude and frequency changes of mEPSCs in DA-GFP neurons, the average charge transfer of mEPSCs was significantly increased in DA-GFP neurons (334±93 vs 100±20%; n=8; P<0.01; U-test) (Fig. 2F).

The GABA miniature inhibitory postsynaptic currents (mIPSCs) were also recorded from the same GFP and DA-GFP neurons (Fig. 3A) used for mEPSC recordings. Surprisingly, the effects of DA-GFP overexpression on GABA transmission were more severe than those on glutamate transmission. In neurons overexpressing DA-GFP, cumulative probability plots of mIPSC amplitude were significantly shifted to lower values compared with those of GFP neurons (n=8; P<0.01; K-S test) (Fig. 3B). The average amplitude of mIPSCs was lower in DA-GFP neurons (24.0±0.9 pA) than in GFP neurons (34.3±1.8 pA) (Fig. 3B, inset). However, the cumulative probability plots of mIPSC frequency in DA-GFP neurons were significantly shifted to higher values compared with those of GFP neurons (n=8; P<0.001; K-S test) (Fig. 3C). The average frequency of mIPSCs was higher in neurons overexpressing

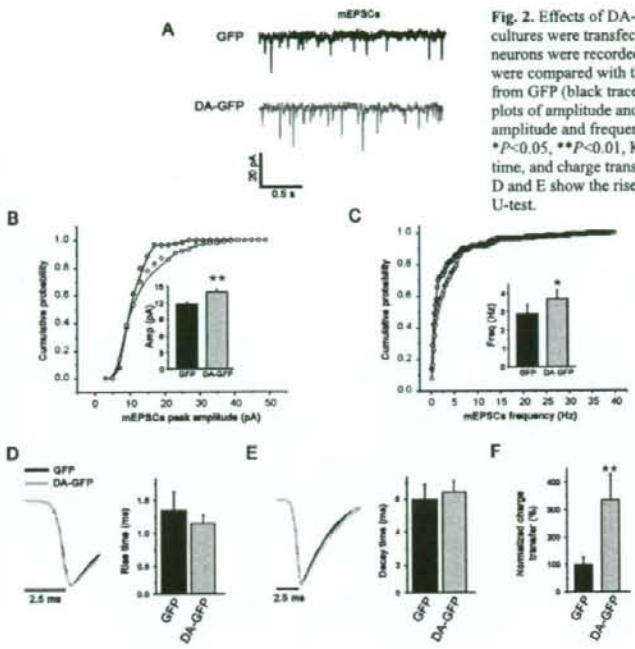

Fig. 2. Effects of DA-GFP overexpression on glutamate function. Mixed hippocampal cultures were transfected at 21 DIV with GFP or DA-GFP, and 1 day later, the transfected neurons were recorded. Electrophysiological recordings of GFP neurons used as controls were compared with those of DA-GFP neurons. (A) Examples of mEPSCs recordings from GFP (black trace) and DA-GFP neurons (gray trace). (B,C) Cumulative probability plots of amplitude and frequency of mEPSCs in GFP and DA-GFP neurons. The average amplitude and frequency of mEPSCs in GFP and DA-GFP neurons are shown as insets. *P<0.05, **P<0.01, K-S test. (D-F) Histograms showing the average rise time, decay time, and charge transfer of mEPSCs respectively in GFP and DA-GFP neurons. Traces in D and E show the rise and decay time, respectively, of the average mEPSCs. **P<0.01, U-test.

DA-GFP (2.8±0.3 Hz) than in GFP neurons (1.3±0.2 Hz; n=8) (Fig. 3C, inset). The average rise time of mIPSCs was significantly increased in DA-GFP neurons (4.28±0.64 mseconds) when compared with that of GFP neurons (1.84±0.16 mseconds; n=8; P<0.05; Student's t-test) (Fig. 3D), whereas the average decay time was significantly decreased (18.93±1.46 vs 23.38±2.41 mseconds; n=8; P<0.05; Student's t-test) (Fig. 3E). However, despite the mIPSC properties changes described above, the average charge transfer in neurons overexpressing DA-GFP (132±33%) was not significantly different from that of GFP neurons (100±3%; n=8; P=0.23; U-test) (Fig. 3F).

Thus, the overexpression of DA-GFP displayed differential effects on functional properties of excitatory and inhibitory synapses. Indeed, DA enhances the strength of excitatory synaptic transmission preferentially (Fig. 2F), without affecting the efficacy of inhibitory synaptic transmission (Fig. 3F). As a result, the average inhibition to excitation charge transfer ratio was significantly reduced in DA-GFP neurons (5.5±0.2) when compared with that of GFP neurons (11.2±0.5; n=8; P<0.01; U-test) (Fig. 3G).

The effects of DA-GFP on synaptic proteins

The changes in GABA and glutamate miniature postsynaptic current (mPSC) properties induced by DA-GFP prompted us to examine whether the density of glutamate and GABA receptors were affected. The quantitative analysis revealed that DA overexpression did not modify significantly the average current density [amplitude (pA)/cell capacitance (pF)] of the agonist-mediated responses compared with that of GFP neurons, which were used as a control (isoguvacine, 8.9±1.8 vs 8.7±2.2, P=0.93; AMPA, 3.9±2.1 vs 6.3±3.7, P=0.39; NMDA, 2.2±0.6 vs 1.8±0.3; n≥9; P=0.37; Student's t-test) (Fig. 4B). These results suggested that the density of $GABA_A$, AMPA, and NMDA membrane receptors were comparable in both GFP and DA-GFP neurons.

We therefore assessed whether postsynaptic expression of DA-GFP might affect the density of glutamatergic and GABAergic presynaptic terminals (Fig. 4C). These terminals were identified with synaptophysin (the general presynaptic marker) or transmitter-specific markers of glutamatergic and GABAergic axons (vGlut1 and Gad-65, respectively). The average densities of synaptophysin and vGlut1 clusters (clusters/10 µm) along dendrites (shafts and/or protrusions) of DA-GFP were not different from those of GFP neurons (syn, 1.1±0.4 vs 1.2±0.4, P=0.7; vGlut1, 3.9±0.4 vs 3.9±0.4, P=0.87; n≥32 dendrites; Student's t-test) (Fig. 4J). However, in DA-GFP neurons, most protrusions (over 98%) were associated with clusters of synaptophysin or vGlut1, suggesting that the majority of protrusions had a presynaptic partner, similar to spines of GFP neurons. Since DA-GFP increased the dendritic spine density and the glutamatergic synaptic activity, we concluded that the density of glutamatergic synapses was increased in DA-GFP neurons.

The postsynaptic expression of DA-GFP did not affect the density of GABA presynaptic terminals in DA-GFP versus GFP neurons (Gad-65, 1.1±0.3 vs 1.2±0.5 clusters/10 µm; n≥32 dendrites; P=0.55; Student's t-test) (Fig. 4J). We next assessed whether the density of GABA synapses was affected in DA-GFP neurons. For this purpose we used β2,3 subunits of the $GABA_A$ receptor as a postsynaptic marker because β2,3 is one of the most abundant subunits of the $GABA_A$ receptors in the brain (McKernan and Whiting, 1996). Our data showed that the average density of clusters (clusters/10 µm) positive for β2,3 or for synaptophysin and β2,3 in DA-GFP was not different from that of GFP neurons (β2,3, 4.8±0.8 vs 4.5±0.8, P=0.51; β2,3 + syn, 1.4±0.5 vs 1.7±0.5, P=0.29; n≥32 dendrites; Student's t-test) (Fig. 4J). Therefore the densities of GABA terminals and synapses were similar in GFP and DA-GFP neurons. Taken together, these data indicated that the ratio of glutamatergic to GABAergic synapses was increased in DA-GFP neurons.

One possible explanation of the absence of significant changes in the density of presynaptic terminals in the presence of such marked changes in the density and shape of postsynaptic spines is that multiple spines can share the same terminal. If this is the case, multiple active zones should form, with a corresponding increase of active zone-associated proteins, such as bassoon. To assess this hypothesis, we studied the effects of DA overexpression on bassoon clusters (Fig. 5A,B‴). Our data showed that the average density of bassoon clusters (clusters/10 µm) along dendrites (shafts and/or protrusions) was increased in DA-GFP (28.2±1.9) compared with that of GFP neurons (16.8±2.0; n≥15 dendrites, P<0.0001; Student's

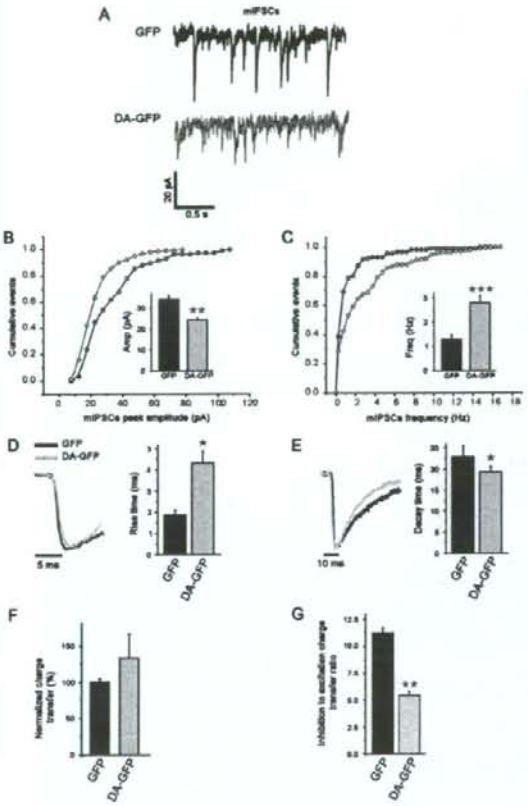

Fig. 3. Effects of DA-GFP overexpression on GABA function. Mixed hippocampal cultures were transfected at 21 DIV with GFP or DA-GFP, and 1 day later, the transfected neurons were recorded. Electrophysiological recordings of GFP neurons used as controls were compared with those of DA-GFP neurons. (A) Examples of mIPSCs recordings from GFP neurons (black trace) and DA-GFP neurons (gray trace). (B,C) Cumulative probability plots of amplitude and frequency of mIPSCs in GFP and DA-GFP neurons. The average amplitude (B) and frequency of mIPSCs (C) in GFP and DA-GFP neurons are shown in insets. $^{**}P<0.01$, $^{***}P<0.001$, K-S test. (D-G) Histograms showing the average rise time, decay time, charge transfer and inhibition to excitation transfer charge ratio of mEPSCs, respectively, in GFP and DA-GFP neurons. $^{*}P<0.05$, *t*-test; $^{**}P<0.01$, U-test.

t-test) (Fig. 5C). Moreover, the average number of bassoon clusters on spines was increased almost twofold in DA-GFP neurons (1.9±0.2 vs 1.0±0.1 clusters/spine; $n\geqslant15$ dendrites; $P<0.0001$; Student's *t*-test) (Fig. 5D). From these data, we concluded that indeed the increased number of spines was paralleled by an increase in the number of active zones.

Effects of downregulation of DA expression on synaptic function

Western blot analysis showed that treatment of mature mixed hippocampal cultures with DA antisense oligonucleotides (AS), whose specificity and efficiency have been described previously (Takahashi et al., 2003; Takahashi et al., 2006), reduced significantly the expression of endogenous DA (AS, 11.87±3.47%) when compared with untreated (Ctl, 100.00±14.77%; $n=7$; $P<0.0001$; Bonferroni's test) or sense-treated neurons (S, 84.59±12.91%; $n=7$; $P<0.001$; Bonferroni's test) (Fig. 6A,B, right panel). The expression of another neuronal protein such as β3-tubulin was not altered by oligonucleotide treatments when compared with untreated or sense-treated cultures (Ctl, 100.00±1.15%; S, 100.17±1.84%; AS, 100.21±1.68%; $n=7$; $P=0.99$; ANOVA) (Fig. 6A,B, left panel), in keeping with previously reported data for β-actin (Takahashi et al., 2003; Takahashi et al., 2006).

Whole-cell recordings of spontaneous and miniature synaptic currents were performed on mature cultured hippocampal neurons treated with sense oligonucleotides (used as a control, for details see supplementary material Fig. S4) or antisense oligonucleotides. Both sense and antisense oligonucleotide-treated neurons showed spontaneous activity (Fig. 6C), suggesting that these neurons were alive and fully integrated in the neuronal network. In addition, the neuronal network activity was not affected by the treatment with antisense oligonucleotides compared with that of neurons treated with sense oligonucleotides. Indeed, the average charge transfer of sPSCs was not significantly different in both culture types (S, 100±15%; AS, 92±21%; $n\geqslant6$; $P=0.8$; U-test) (Fig. 6D).

The mEPSCs were recorded from S or AS neurons (Fig. 7A). In antisense-treated neurons, the cumulative probability plots of amplitude and frequency of mEPSCs were significantly shifted to lower values when compared to sense-treated neurons ($n=6$; $P<0.05$; K-S test) (Fig. 7B,C). The average amplitude and frequency of mEPSCs were decreased in antisense-treated neurons (11.3±0.9 pA; 4.3±1.5 Hz) when compared with those of sense-treated neurons (12.3±1.0 pA; 6.7±2.1 Hz) (Fig. 7B,C, insets). However, the average rise times (S, 1.44±0.16; AS, 1.58±0.15; $n=6$; $P=0.67$; Student's *t*-test) (Fig. 7D) and decay times (S, 4.42±0.65; AS, 4.67±0.61; $n=6$; $P=0.14$; Student's *t*-test) were comparable (Fig. 7E). As a result of amplitude and frequency changes of mEPSCs in antisense-treated neurons, the average charge transfer of mEPSCs was significantly reduced (56±3 vs 100±15%; $n=6$; $P<0.05$; U-test) (Fig. 7F).

We recorded the GABA mIPSCs from the same oligonucleotide-treated neurons, where the mEPSCs were recorded (Fig. 8A). In antisense-treated neurons, the cumulative probability plots of amplitude and frequency of mIPSCs were significantly shifted to lower values as compared with those of sense-treated neurons ($n=6$; $P<0.01$ for the amplitude and $P<0.05$ for the frequency; K-S test) (Fig. 8B,C). The average amplitude and frequency of mIPSCs were decreased in antisense-treated (15.9±1.6 pA; 2.3±0.7 Hz) when compared to sense-treated neurons (23.2±2.0 pA; 3.1±0.7 Hz) (Fig. 8B,C, insets). The average rise time and decay time of mIPSCs were not significantly modified in antisense-treated (3.52±0.44 mseconds; 20.48±1.78 mseconds) when compared with those of sense-treated neurons (2.74±0.31 mseconds; 22.25±3.30 mseconds; $n=6$; $P=0.12$ and 0.37 respectively; Student's *t*-test) (Fig. 8D,E). Owing to the mIPSC property changes described above, the average charge transfer in antisense-treated neurons was significantly reduced (78±11 vs 100±10%; $n=6$; $P<0.05$; U-test) (Fig. 8F). Thus, the reduction of DA expression affected both the functional properties of glutamatergic and GABAergic synapses. Despite these changes, the inhibition to excitation charge transfer ratio was not altered by the reduction of DA expression (AS, 7.7±2.8; S, 5.1±1.5; $n=6$; $P=0.9$; U-test) (Fig. 8G). Thus, the functional balance between excitation and inhibition was maintained while DA level was reduced.

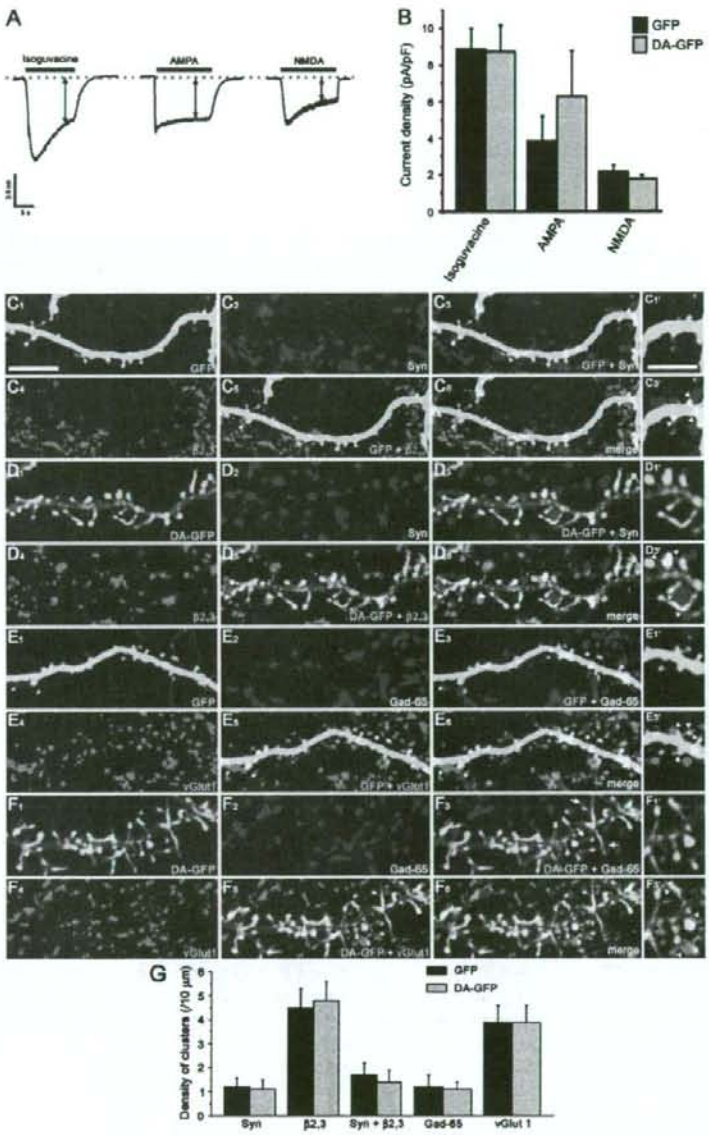

Fig. 4. Effects of DA-GFP on the density of GABA and glutamate receptors and synaptic proteins. Transfected neurons were recorded in whole-cell configuration at –60 mV for $GABA_A$- or AMPA-generated responses and –20 mV for NMDA-mediated current in the presence of TTX and strychnine. (A) Example of current responses induced by bath application of receptor agonists, Isoguvacine (20 µM), AMPA (100 µM) and NMDA (50 µM, with 10 µM glycine, NMDA coactivator) to activate $GABA_A$, AMPA and NMDA receptors, respectively, 10 seconds after starting perfusion (double arrows) with agonist-containing solution. (B) Quantitative analysis revealed that DA overexpression did not modify significantly the average current density of the agonist-mediated responses compared with that of GFP neurons. (C) Mixed hippocampal cultures were transfected at 21 DIV with GFP (C_1,E_1 and insets $C_{1'}$,$E_{1'}$) or DA-GFP (D_1,F_1 and insets $D_{1'}$,$F_{1'}$), and 1 day after transfection, cells were double immunostained for synaptophysin (C_2,D_2) and the subunit β2,3 of $GABA_A$ receptors (C_4,D_4) or for Gad-65 (E_2,F_2) and vGlut1 (E_4,F_4). All the synaptic markers were located either on the dendritic shafts or on dendritic protrusions. Interestingly, we observed in DA neurons that several dendritic spines share the same presynaptic terminal (see arrowheads in $D_{3'}$ vs $C_{3'}$ and $F_{3'}$ vs $E_{3'}$). Scale bars: 10 µm in C_1-F_6 and 5 µm in insets in right column. (G) The average density of syn, β2,3, syn + β2,3, Gad-65 and vGlut1 clusters along dendrites of DA-GFP were not different from those of GFP neurons. Note that in addition to dendrites of transfected neurons, all synaptic markers also stained dendrites of nontransfected neurons.

Discussion

This study provides the first evidence that DA can modulate both glutamatergic and GABAergic synaptic activities through regulation of spine plasticity.

Actin-binding domain of drebrin A is involved in spine plasticity

Our data clearly demonstrate that overexpression of DA increases spine density in mature hippocampal neurons. This finding is in keeping with the work of Takahashi and colleagues (Takahashi et al., 2003; Takahashi et al., 2006), who showed that downregulation of DA by antisense oligonucleotide treatment significantly decreased the density of filopodia spines. Altogether, these data strongly suggest that DA is involved in spine formation. The modification of the dynamic turnover of dendritic spines by stabilisation of F-actin might be one of the possible mechanisms leading to increased spine density. Indeed, we show that DA overexpression in CHO-K1 cells protects F-actin from cytochalasin B destabilization (supplementary material Fig. S3). Consistent with these findings, earlier studies also showed that DA expression in fibroblasts induced cytochalasin-D-resistant actin structures at their adhesion

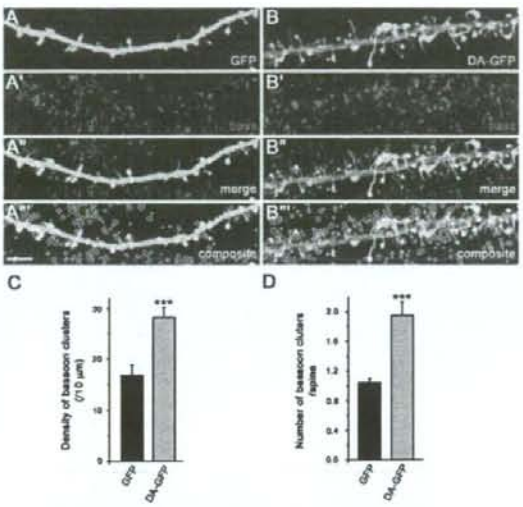

Fig. 5. Effects of DA-GFP overexpression on bassoon protein. Mixed hippocampal cultures were transfected at 21 DIV with GFP (A) or DA-GFP (B) and 1 day after transfection, cells were immunostained for bassoon (A′,B′). (A″ and B″) Merge of panels A and A′ and B and B′, respectively. (A‴ and B‴) Composite of A″ and B″, and drawings showing selected objects obtained with ImageJ software from A′ and B′, respectively. (C,D) Histograms showing the density of bassoon clusters (C) and their number per spine (D) in GFP and DA-GFP neurons. ***P<0.0001, Student's t-test. Scale bar: 5 µm.

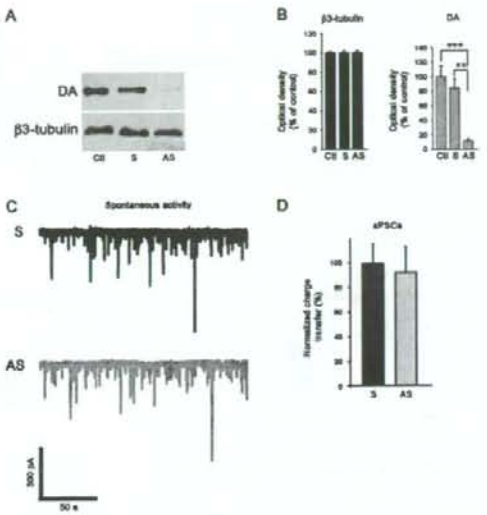

Fig. 6. Effects of DA downregulation on network activity. Mixed hippocampal cultures of 21 DIV treated for 2 days in the absence (untreated) or the presence of 10 µM sense (S) or antisense (AS) oligonucleotides. Following treatment, the cells were either used for western blot analysis (A,B) or electrophysiology recordings (C,D). **P<0.001, Bonferroni's test. (C) Using whole-cell recordings, sPSCs were detected at −60 mV in sense- (black trace) and antisense-treated neurons (gray trace). (D) Histogram showing the sPSC average charge transfer in all recorded neurons.

plaques (Ikeda et al., 1996). It is thus possible that elevated DA levels stabilize actin filaments in spines and alter their dynamic turnover (retraction). This inhibition of spine retraction by DA might lead to the increase in spine density.

In addition, our data show that DA regulates spine shape and size. Indeed, DA-GFP overexpression in mature cultured hippocampal neurons caused elongation of dendritic spines, which were similar to the spines observed in GFP-DA-expressing cortical neurons (Hayashi and Shirao, 1999). Furthermore, DA-GFP increases spine head width. This finding is corroborated by studies showing that downregulation of DA significantly decreases the width of filopodia spines (Takahashi et al., 2006). The morphological changes of dendritic spines induced by DA-GFP are mediated by its actin-binding domain as illustrated by our data (see Fig. 1A-G).

It has been reported that drebrin interacts directly with profilin (Mammoto et al., 1998), an actin-binding protein, known to stimulate actin polymerization (Carlsson et al., 1977; Buss et al., 1992; Rothkegel et al., 1996). One possible mechanism to induce morphological changes of dendritic spines is that DA recruits profilin to stimulate actin polymerization, leading to the elongation and increase in size of dendritic spines.

It has also been shown that DA reduced the movement of actin over a myosin-bound surface in the sliding actin motility assay, and inhibited the actin-based ATPase activity of myosin (Hayashi et al., 1996). The actomyosin-based machinery might thus be another mechanism involved in the elongation of spines. Based on these observations, we suggest that elongation of spines induced by DA-GFP may result from the superimposition of two additive mechanisms: polymerization of actin and inhibition of actomyosin activity and that DA is a key protein in the plasticity of dendritic spines.

DA modulates glutamatergic and GABAergic synaptic transmission

Our data showed that the long protrusions induced by DA are associated with presynaptic glutamatergic terminals. Despite the increased spine density (by about 43%), the density of glutamatergic terminals is not modified. However, the average number of active zone-associated bassoon clusters on spines is increased twice. Since bassoon is a component of the presynaptic apparatus of both excitatory glutamatergic and inhibitory GABAergic synapses (Richter et al., 1999), the increase of bassoon clusters suggests that at least some of the dendritic spines share the same glutamatergic terminal. Consistent with this idea, a single glutamatergic terminal could be contacted by two DA dendritic spines (see arrowheads in Fig. 4). As a result, the density of glutamatergic synapses is increased. Furthermore, our electrophysiological data demonstrate that these synapses are functional and more active. Indeed, an increase in the frequency (~27%) and amplitude (~18%) of mEPSCs were observed in DA-GFP neurons. The frequency increase could result from the augmented number of functional excitatory synapses, whereas the amplitude increase could be due to spine head widening (~13%) and/or to simultaneous glutamate release at multiple active sites. Bath application of glutamatergic agonists showed that overall density of receptors is preserved in DA-GFP neurons. This method does not permit us to distinguish the response mediated by extrasynaptic receptors from that mediated by synaptic receptors.

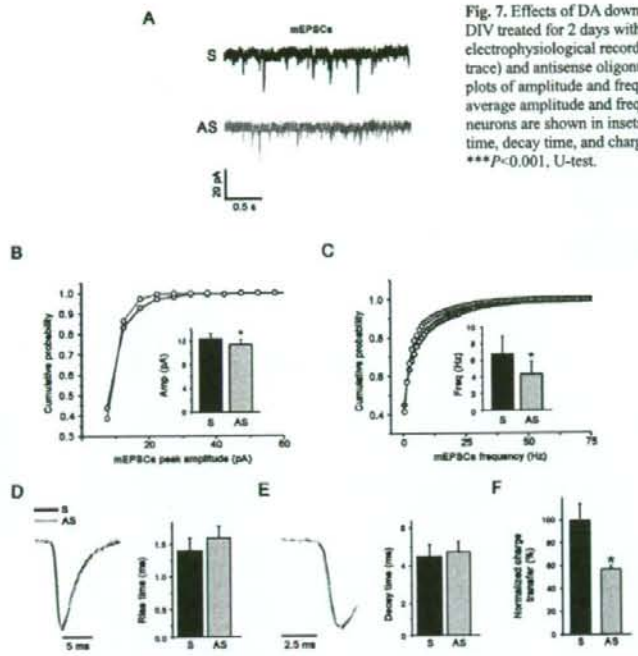

Fig. 7. Effects of DA downregulation on glutamate function. Mixed hippocampal cultures of 21 DIV treated for 2 days with 10 μM sense or antisense oligonucleotides, followed by electrophysiological recording. (A) Examples of mEPSCs recordings from DA sense (black trace) and antisense oligonucleotide-treated neurons (gray trace). (B,C) Cumulative probability plots of amplitude and frequency of mEPSCs in sense- and antisense-treated neurons. The average amplitude and frequency of mEPSCs in sense and antisense oligonucleotide-treated neurons are shown in insets. *P<0.05, K-S test. (D-F) Histograms showing the average rise time, decay time, and charge transfer of mEPSCs in oligonucleotide-treated neurons. ***P<0.001, U-test.

Therefore, these results show that overall density of glutamatergic membrane receptors (extrasynaptic and synaptic) was comparable in both GFP and DA-GFP neurons. Thus, the increased amplitude of mEPSCs could be explained by the spine head widening and the redistribution of glutamatergic extrasynaptic receptors to synaptic sites. The fact that the mEPSC kinetics was comparable in GFP and DA-GFP neurons, suggests that the subunit composition of glutamate receptors was not different in the newly formed and the already established excitatory synapses of DA neurons.

Despite a 43% increase in the density of excitatory synapses in DA-GFP neurons, we did not observe an equivalent increase in mEPSC frequency. This could suggest that synapses on dendritic shafts move on newly formed spines and/or that some of the DA-GFP excitatory synapses are inactive. In both cases, DA-GFP overexpression resulted in a significant increase in excitatory synaptic activity. As a result of the amplitude and frequency changes of mEPSCs in DA-GFP neurons, the glutamatergic transmission efficacy was significantly increased in DA-GFP compared with that of GFP neurons.

Our data revealed that although the mIPSC properties change (frequency, amplitude, and kinetics), the GABAergic transmission efficacy in DA-GFP neurons was not significantly different. The possible mechanisms that mediate the effect of DA on GABA postsynaptic activity are unknown. However it is interesting that DA could interact with gephyrin, a $GABA_A$ receptor anchoring protein (Kneussel and Loebrich, 2007), through profilin (Mammoto et al., 1998). Immunocytochemical data showed that the density of GABA synapses was also similar in GFP and DA-GFP neurons. As a result, the average inhibition to excitation charge transfer ratio is significantly reduced in DA-GFP neurons. Altogether, these observations indicate that DA-GFP overexpression increases the density of excitatory relative to inhibitory synapses, and enhances the excitation to inhibition ratio. The excitatory to inhibitory synapse ratio is believed to be crucial for normal neuronal computation and is generally kept constant by homeostatic mechanisms (Burrone et al., 2002; Hausser et al., 2000; Knott et al., 2002; Liu, 2004; Turrigiano and Nelson, 2004). Some of the factors that control the overall change in the ratio of excitatory-inhibitory synapse number and activity have only recently been discovered. Several studies have implicated the synaptic cell adhesion molecules called neuroligin (NLG) proteins and the scaffolding postsynaptic density protein PSD-95 (Prange et al., 2004; Chih et al., 2005; Levinson et al., 2005; Levinson and El Husseini, 2005a; Levinson and El Husseini, 2005b). An alteration in the excitation-inhibition synaptic balance was also suggested to occur in several neurodevelopmental psychiatric disorders, including autism and some forms of mental retardation (Rubenstein and Merzenich, 2003; Levinson and El Husseini, 2005a; Levinson and El Husseini, 2005b). The importance of our findings is emphasized by the recent discovery that the drebrin level is increased in the superior frontal cortex in neurological disorders accompanied by mild cognitive impairment (MCI) (Counts et al., 2006; Kojima and Shirao, 2007). It has been suggested that this might be a compensatory reaction to the reduced synaptic function in MCI.

Since overexpression of DA affected the glutamate and GABA synaptic properties, we investigated the functional consequences of a reduced DA expression. In DA-knockdown neurons, both amplitude and frequency of mEPSCs were reduced. The decreased amplitude of mEPSCs could be explained by the decreased in the width of filopodia spines observed in DA-knockdown neurons (Takahashi et al., 2006). The decreased frequency of mEPSCs in DA-knockdown neurons could be due to the decreased number of functional excitatory synapses. This possibility is supported by the fact that DA-knockdown neurons displayed a significant decrease in the density of filopodia spines (Takahashi et al., 2003; Takahashi et al., 2006). Similarly to mEPSCs, the frequency and amplitude of mIPSCs were also reduced in DA-knockdown neurons. These decreases could be due to the loss of dendritic spines containing functional inhibitory synapses (see arrows in Fig. 4F). Spines receiving both an excitatory and inhibitory input were first described by Jones and Powell (Jones and Powell, 1969) in the cat somatosensory cortex, and have since been implicated in inhibitory mechanisms by which the inhibitory synapses can reduce the excitatory influence of other synapses (Dehay et al., 1991; Knott et al., 2002). The fact that the kinetics of mEPSCs and mIPSCs were not affected by DA knockdown, suggests that the subunit composition of the glutamate and GABA receptor channels were not different in residual glutamatergic and GABAergic synapses, respectively, of DA-knockdown neurons. The parallel effects

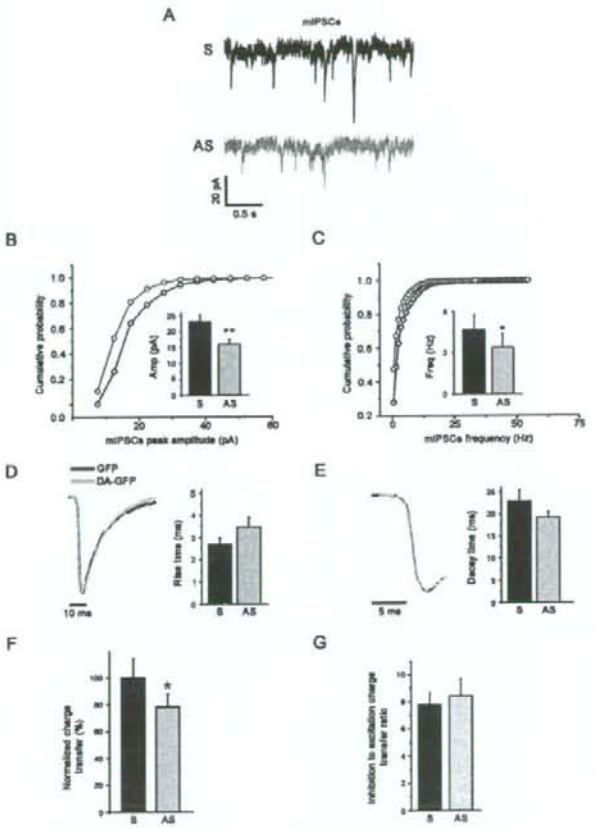

Fig. 8. Effects of DA downregulation on GABA function. Mixed hippocampal cultures of 21 DIV treated for 2 days with 10 μM sense (S) or antisense (AS) DA oligonucleotides, followed by electrophysiological recording. (A) Examples of mIPSC recordings from sense (black trace) and antisense neurons (gray trace). (B,C) Cumulative probability plots of amplitude and frequency of mIPSCs in sense and antisense oligonucleotide-treated neurons. The average amplitude and frequency of mIPSCs in oligonucleotide-treated neurons are shown in insets. *P<0.05, **P<0.01, K-S test. (D-G) Histograms showing the average rise time, decay time, charge transfer and inhibition to excitation charge transfer ratio of mIPSCs in oligonucleotide-treated neurons. ***P<0.001, U-test.

exerted by DA knockdown on mEPSCs and mIPSCs resulted in the reduction of both glutamatergic and GABAergic transmission efficacy. Despite these changes, the inhibition to excitation ratio was not affected by the 73% reduction of DA expression. Combined with the data described above, these results indicated that the residual DA was not sufficient to affect the functional balance between excitation and inhibition. One possible explanation of the effects of DA on the inhibitory to excitatory ratio is that in the case of overexpression of DA we affect only transfected postsynaptic neurons, whereas in the case of underexpression of DA we also affect the presynaptic neurons. Thus, the amounts of DA available can contribute to the homeostatic mechanism that maintains the structural and functional balance between excitatory and inhibitory synapses.

Interestingly, a decreased level in DA content is reported in the superior temporal cortex in MCI and Alzheimer disease (Counts et al., 2006; Kojima and Shirao, 2007). In addition, the level of postsynaptic DA has been shown to strongly correlate with the severity of cognitive impairment (Counts et al., 2006; Kojima and Shirao, 2007). This indicated that a critical level of DA protein might be required for normal function. Therefore, we propose a model in which improper expression of DA might trigger either an imbalance in neuronal excitability or an alteration in synaptic transmission. In both cases, these alterations result in synaptic dysfunction reminiscent of that observed in the cognitive impairment accompanying normal aging and neurological disorders, including Alzheimer disease (Harigaya et al., 1996; Hatanpää et al., 1999; Counts et al., 2006; Kojima and Shirao, 2007) and Down syndrome (Shim and Lubec, 2002).

In conclusion, the identification of factors involved in synaptogenesis should enhance our understanding of the mechanisms responsible for synaptic plasticity as well as the cellular and molecular defects observed in neurological disorders.

Materials and Methods

cDNA constructs

The full-length drebrin A (DA, NCBI accession number NM-031024) fragment was amplified by PCR and inserted into pEGFP-N1 vector (BD Bioscience Clontech, Palo Alto, CA). The DA-GFP construct was subsequently fully sequenced. We also used GFP-ABS and GFP-DAΔABS constructs (see Hayashi et al., 1999).

Cell lines, transfection and immunofluorescence

Chinese Ovary (CHO-K1) cells were obtained from the American Type Tissue Culture Collection (ATCC, Molsheim, France). They were grown in F12 (Invitrogen, Cergy Pontoise, France), supplemented with 10% fetal bovine serum (FBS, Invitrogen), 2 mM glutamine (Invitrogen), 100 U/ml penicillin and 100 mg/ml streptomycin (Sigma, Lyon, France). Cells were rinsed one time with serum-free medium (Opti-MEM, Invitrogen) and transfections were performed according to the manufacturer's protocol (Invitrogen). Briefly, cells were incubated in a solution containing 500 μl Opti-MEM, 4 μl Plus reagent, 6 μl lipofectamine reagent (Invitrogen) and 1 μg of either the GFP, the DA-GFP, the GFP-ABS or the GFP-DAΔABS construct. After incubation for 4 hours at 37°C, the transfection mixture was replaced by a fresh complete growth medium containing 10% FBS. 24 hours after transfection, cells were fixed with 4% paraformaldehyde (PFA) in 0.12 M phosphate buffer (PB), pH 7.2-7.4 for 20 minutes at room temperature (RT).

Quantitative analyses of the number of transfected cells were performed using a fluorescence microscope with a ×20 objective. Twenty fields per coverslip per experiment (n=3) were analyzed. Data were expressed as mean % of total cells per experiment ± s.e.m.

For the F-actin staining, the cells were incubated with 0.5% Triton X-100 and 1% blocking reagent (BR, Roche, Meylan, France) for 30 minutes and exposed for 2 hours at RT to 0.5 U per coverslip of Texas-Red-labeled X phalloidin (Molecular Probes, Leiden, Netherlands), rinsed in PB and incubated with 0.5 μg/ml DNA intercalant Hoechst 33258 (Molecular Probes). Cells were rinsed in PB and then mounted with Fluoromount G (Electron Microscopy, Fort Washington, PA).

In some experimental sets (n=3), the microfilament-depolymerizing drug cytochalasin B (Sigma, used at 10 μg/ml final concentration in 0.1% dimethylsulfoxide) was added into the medium to assess the stability of F-actin of transfected cells. After incubation with cytochalasin B for 10 minutes, cells were fixed with PFA for 20 minutes, washed three times with PB, stained for F-actin as described above, rinsed in PB, then incubated with Hoechst 33258, and mounted with Fluoromount G.

Analysis was performed on a Leica (Mannheim, Germany) TCS SP2 confocal microscope using the 488 nm band of an Ar laser and the 543 nm band of a He-Ne laser for excitation of GFP and Texas Red, respectively. Images were acquired by sequential scanning using ×63 1.32 oil-immersion lens (zoom 3) and processed with Adobe Photoshop. Results are shown in supplementary material Figs S1-S4.

Primary cultures of rat hippocampal neurons and transfection

Mixed hippocampal cultures were prepared from embryonic day 18 (E18) rats according to Rami et al. (Rami et al., 2006). At 21 DIV, mixed hippocampal cultures were transiently transfected using a Magnetofection Kit (OZ Biosciences, Marseille, France) and lipofectamine 2000 reagent according to the OZ Biosciences protocol. Following transfection, the cells were either used for electrophysiology recordings or fixed with 4% PFA in 0.12 M phosphate buffer (PB), pH 7.2-7.4 for 20 minutes at RT for immunofluorescence. The transfection efficiency was less than 1%.

Immunofluorescence

For single immunolabeling of DA and double immunolabeling of DA/synaptophysin and DA/PSD-95, mixed hippocampal cultures of 21 DIV were incubated overnight at RT in DA antiserum (1:500) (Aoki et al., 2005) or a mixture of DA antiserum and either synaptophysin (1:300, Chemicon, Temecula, CA), or PSD-95 (1:500, Upstate, Charlottesville, VA) monoclonal antibodies diluted in PB containing 1% BR. After several rinses in PB, coverslips were incubated in a mixture of Alexa 488-conjugated goat anti-rabbit IgG and Cy3-conjugated goat anti-mouse IgG (1:200, both from Jackson Immunoresearch, West Grove, PA) diluted in PB containing 1% BR.

For double labeling of DA/F-actin, cells were exposed for 2 hours at RT to 0.5 U per coverslip of Texas-Red X phalloidin prepared in PB containing 1% BR.

Single immunolabeling of bassoon, double immunolabeling of synaptophysin/β2,3 or Gad-65/vGlut1 were performed on hippocampal neurons transfected with GFP or DA-GFP. Cells were incubated with the following primary antibodies (most from Chemicon): polyclonal synaptophysin (1:500) and mouse monoclonal antibody against $GABA_A$ receptor beta chain (β2,3, 1:500) or mouse monoclonal antibody against Gad 65 (one of the glutamic acid decarboxylase isoforms, 1:300) and guinea pig polyclonal antiserum against vGlut1 (vesicular glutamate transporter 1, 1:5000) or mouse monoclonal antibody against bassoon (1:300, Assay designs, Ann Arbor, MI). After several rinses in PB, coverslips were incubated for 1 hour at RT in biotinylated goat- anti-rabbit IgG (1:200) or anti-mouse IgG (1:200), and then incubated in a mixture of Cy5-conjugated streptavidin and Cy3-conjugated goat anti-mouse IgG or Cy3-conjugated donkey anti-guinea pig IgG (1:200, all from Jackson Immunoresearch). Bassoon staining was revealed with Alexa Fluor 594-conjugated goat anti-mouse IgG (1:200, Molecular Probes) diluted in PB containing 1% BR. In all cases, no labeling was detected when specific antibodies were replaced with normal rabbit, mouse, guinea pig serum or when primary antibodies were omitted.

Image acquisition and quantification

All measurements were performed on spiny and pyramidal neurons that were visually identified based on their morphology (Benson et al., 1994). Images were acquired with an Olympus fluoview-500 confocal microscope (Olympus, France) using an oil immersion ×60 1.4 lens (zoom 3). Dendritic protrusions were reconstructed from 7 to 15 serial images of 0.5 μm thickness projected onto one plane. For morphometric analysis, protrusion length, width and density were measured from projected images using Neurolucida software as described previously (Rami et al., 2006).

Analysis of synaptic proteins was performed with an Olympus Fluoview-500 confocal microscope using the 488, 543, 633 laser lines for excitation of GFP, Cy3 and Cy5, respectively. For quantitation of synaptic protein clusters, pictures from GFP and DA-GFP neurons were taken sequentially using ×63 1.4 (zoom 3) with the same exposure parameters. Then the projections of z-stacks were thresholded equally to eliminate the background of dendritic staining and the remaining clusters were counted based on their location either on dendritic shafts or on dendritic protrusions using Neurolucida or ImageJ softwares. Five to ten transfected neurons were chosen randomly from three independent experiments for GFP and DA-GFP constructs and the number of clusters was collected from at least three dendritic segments of 100 μm per neuron. Then, the density of the synaptic protein clusters was determined similarly to protrusion density.

Westerns blot analysis

For western blot analysis, cultures were homogenized in 50 mM Tris-HCl, pH 6.8, 5% SDS, 6% 2-mercaptoethanol, 10% glycerol and 4 mM EDTA. Protein samples were boiled for 10 minutes, and equal amounts were loaded into each well, resolved on 8% SDS-polyacrylamide gels and transferred onto Hybond-ECL nitrocellulose membranes (Amersham Biosciences, Germany). Blots were then blocked, immunostained with appropriate antibodies and immunodetected using the enhance chemiluminescence system (ECL, Amersham Biosciences). Chemiluminescent signals were projected on X-ray film and digitalized, and the signals were quantified using ImageJ.

Antisense experiments

Translation of DA was suppressed by treatment of cultures with an antisense phosphorothioate-substituted DNA oligonucleotides (AS) (Takahashi et al., 2006). The sense phosphorothioate oligonucleotide (S) (Takahashi et al., 2006) was used as negative control since the sense oligo treatment has no effect on the expression of DA, β3-tubulin and synaptic activity compared with untreated cultures (supplementary material Fig. S4). Therefore, we used sense oligo-treated neurons for the analysis of the control neuronal activity. At 21 DIV, cultures were treated for 2 days in the absence (untreated) or the presence of 10 μM sense or antisense oligonucleotides. Following treatment, the cells were either used for western blot analysis or electrophysiology recordings.

Whole-cell recording

sPSCs or mPSCs were recorded from visually identified spiny and pyramidal neurons (Chudotvorova et al., 2005; Rami et al., 2006). The mEPSCs or mIPSCs were isolated at –60 mV in the presence of TTX, D-AP5, strychnine and bicuculline/CNQX. We took into account for analysis, only neurons in which both mEPSCs and mIPSCs were recorded. To evaluate the change produced by DA-GFP overexpression or by treatment with antisense oligonucleotides against DA on network activity and the overall synaptic strength of a single neuron (Turrigiano et al., 1998; Burrone et al., 2002; Liu, 2004; Chih et al., 2005), the mean charge transfer was determined. This parameter depends simultaneously on the amplitude, frequency and kinetic of postsynaptic currents. Therefore, during spontaneous activity, charge transfer reflects neuronal network activity. When this activity is blocked by TTX, the charge transfer reflects the overall synaptic strength of a single neuron (Liu, 2004). Charge transfers for sPSCs or mPSCs were calculated for each recorded neuron as the sPSCs or mPSCs area (charge transferred by single postsynaptic current) multiplied on instantaneous frequency value (instantaneous frequency=1/inter-event interval). In each experiment, the mean charge transfer values were normalized relative to the average mean control value (expressed in %). To evaluate the effects of postsynaptic receptor agonists within different cells, the current densities (amplitude/cell capacitance) were compared. Amplitudes of currents induced by bath application of agonists were measured 10 seconds after starting perfusion with agonist containing solution (see Fig. 4A).

Statistical analysis

All experiments were repeated at least three times with different culture series. Morphological, immunostaining and western blot data were statistically analyzed by unpaired Student's *t*-test for comparing two groups, or by ANOVA, with *a* post hoc Bonferroni's *t*-test (Bonferroni test) for multiple comparison, as applicable.

Statistical analyses for frequency, amplitude, and area of mPSCs were performed with the nonparametric Kolmogorov-Smirnov (K-S) test. Unpaired Student's *t*-test was used to examine the statistical significance of the differences between groups of others parameters (decay time, rise time, density of agonist induced current). All data parameters were expressed as the mean ± s.e.m. To determine the difference between groups of charge transfer data, Kolmogorov-Smirnov as well as Mann-Whitney U (U-test) tests were used; the higher value of P was taken into account.

We thank Djaffar Boussa, Santiago Rivera, François Feron and Michel Khrestchatisky for critical reading of the manuscript. We also thank Marie-Pierre Blanchard for her help with the Leica laser microscope. This work was supported by grants from the Institut National de la Santé et de la Recherche Médicale (INSERM) and the Centre National de la Recherche Scientifique (CNRS). This project was initiated in the INMED laboratory directed by Yezekiel Ben Ari.

References

Aoki, C., Sekino, Y., Hanamura, K., Fujisawa, S., Mahadomrongkul, V., Ren, Y. and Shirao, T. (2005). Drebrin A is a postsynaptic protein that localizes in vivo to the submembranous surface of dendritic sites forming excitatory synapses. *J. Comp. Neurol.* **483**, 383-402.

Ballestrem, C., Wehrle-Haller, B. and Imhof, B. A. (1998). Actin dynamics in living mammalian cells. *J. Cell Sci.* **111**, 1649-1658.

Benson, D. L., Watkins, F. H., Steward, O. and Banker, G. (1994). Characterization of GABAergic neurons in hippocampal cell cultures. *J. Neurocytol.* **23**, 279-295.

Burrone, J., O'Byrne, M. and Murthy, V. N. (2002). Multiple forms of synaptic plasticity triggered by selective suppression of activity in individual neurons. *Nature* **420**, 414-418.

Buss, F., Temm-Grove, C., Henning, S. and Jockusch, B. M. (1992). Distribution of profilin in fibroblasts correlates with the presence of highly dynamic actin filaments. *Cell Motil. Cytoskeleton* **22**, 51-61.

Carlsson, L., Nystrom, L. E., Sundkvist, I., Markey, F. and Lindberg, U. (1977). Actin polymerizability is influenced by profilin, a low molecular weight protein in non-muscle cells. *J. Mol. Biol.* **115**, 465-483.

Chih, B., Engelman, H. and Scheiffele, P. (2005). Control of excitatory and inhibitory synapse formation by neuroligins. *Science* **307**, 1324-1328.

Chudotvorova, I., Ivanov, A., Rama, S., Hübner, C. A., Pellegrino, C., Ben-Ari, Y. and Medina, I. (2005). Early expression of KCC2 in rat hippocampal cultures augments expression of functional GABA synapses. *J. Physiol.* **566**, 671-679.

Cooper, J. A. (1987). Effects of cytochalasin and phalloidin on actin. *J. Cell Biol.* **105**, 1473-1478.

Counts, S. E., Nadeem, M., Lad, S. P., Wuu, J. and Mufson, E. J. (2006). Differential expression of synaptic proteins in the frontal and temporal cortex of elderly subjects with mild cognitive impairment. *J. Neuropathol. Exp. Neurol.* **65**, 592-601.

Dehay, C., Douglas, R. J., Martin, K. A. and Nelson, C. (1991). Excitation by geniculocortical synapses is not 'vetoed' at the level of dendritic spines in cat visual cortex. *J. Physiol.* **440**, 723-734.

Edson, K., Weisshaar, B. and Matus, A. (1993). Actin depolymerisation induces process formation on MAP2-transfected non-neuronal cells. *Development* **117**, 689-700.
Fifkova, E. and Delay, R. J. (1982). Cytoplasmic actin in neuronal processes as a possible mediator of synaptic plasticity. *J. Cell Biol.* **95**, 345-350.
Fukazawa, Y., Saitoh, Y., Ozawa, F., Ohta, Y., Mizuno, K. and Inokuchi, K. (2003). Hippocampal LTP is accompanied by enhanced F-actin content within the dendritic spine that is essential for late LTP maintenance *in vivo*. *Neuron* **38**, 447-460.
Harigaya, Y., Shoji, M., Shirao, T. and Hirai, S. (1996). Disappearance of actin-binding protein, drebrin, from hippocampal synapses in Alzheimer's disease. *J. Neurosci. Res.* **43**, 87-92.
Harris, K. M. and Kater, S. B. (1994). Dendritic spines: cellular specializations imparting both stability and flexibility to synaptic function. *Annu. Rev. Neurosci.* **17**, 341-371.
Hatanpaa, K., Isaacs, K. R., Shirao, T., Brady, D. R. and Rapoport, S. I. (1999). Loss of proteins regulating synaptic plasticity in normal aging of the human brain and in Alzheimer disease. *J. Neuropathol. Exp. Neurol.* **58**, 637-643.
Hausser, M., Spruston, N. and Stuart, G. J. (2000). Diversity and dynamics of dendritic signaling. *Science* **290**, 739-744.
Hayashi, K. and Shirao, T. (1999). Change in the shape of dendritic spines caused by overexpression of drebrin in cultured cortical neurons. *J. Neurosci.* **19**, 3918-3925.
Hayashi, K., Ishikawa, R., Ye, L. H., He, X. L., Takata, K., Kohama, K. and Shirao, T. (1996). Modulatory role of drebrin on the cytoskeleton within dendritic spines in the rat cerebral cortex. *J. Neurosci.* **16**, 7161-7170.
Hayashi, K., Ishikawa, R., Kawai-Hirai, R., Takagi, T., Taketomi, A. and Shirao, T. (1999). Domain analysis of the actin-binding and actin-remodeling activities of drebrin. *Exp. Cell Res.* **253**, 673-680.
Ikeda, K., Kaub, P. A., Asada, H., Uyemura, K., Toya, S. and Shirao, T. (1996). Stabilization of adhesion plaques by the expression of drebrin A in fibroblasts. *Brain Res. Dev. Brain Res.* **91**, 227-236.
Ishikawa, R., Hayashi, K., Shirao, T., Xue, Y., Takagi, T., Sasaki, Y. and Kohama, K. (1994). Drebrin, a development-associated brain protein from rat embryo, causes the dissociation of tropomyosin from actin filaments. *J. Biol. Chem.* **269**, 29928-29933.
Ishikawa, R., Katoh, K., Takahashi, A., Xie, C., Oseki, K., Watanabe, M., Igarashi, M., Nakamura, A. and Kohama, K. (2007). Drebrin attenuates the interaction between actin and myosin-V. *Biochem. Biophys. Res. Commun.* **359**, 398-401.
Jones, E. G. and Powell, T. P. (1969). Morphological variations in the dendritic spines of the neocortex. *J. Cell Sci.* **5**, 509-529.
Kneussel, M. and Loebrich, S. (2007). Trafficking and synaptic anchoring of ionotropic inhibitory neurotransmitter receptors. *Biol. Cell* **99**, 297-309.
Knott, G. W., Quairiaux, C., Genoud, C. and Welker, E. (2002). Formation of dendritic spines with GABAergic synapses induced by whisker stimulation in adult mice. *Neuron* **34**, 265-273.
Kojima, N. and Shirao, T. (2007). Synaptic dysfunction and disruption of postsynaptic drebrin-actin complex: a study of neurological disorders accompanied by cognitive deficits. *Neurosci. Res.* **58**, 1-5.
Levinson, J. N. and El-Husseini, A. (2005a). Building excitatory and inhibitory synapses: balancing neuroligin partnerships. *Neuron* **48**, 171-174.
Levinson, J. N. and El-Husseini, A. (2005b). New players tip the scales in the balance between excitatory and inhibitory synapses. *Mol. Pain* **1**, 12.
Levinson, J. N., Chery, N., Huang, K., Wong, T. P., Gerrow, K., Kang, R., Prange, O., Wang, Y. T. and El-Husseini, A. (2005). Neuroligins mediate excitatory and inhibitory synapse formation: involvement of PSD-95 and neurexin-1beta in neuroligin-induced synaptic specificity. *J. Biol. Chem.* **280**, 17312-17319.
Liu, G. (2004). Local structural balance and functional interaction of excitatory and inhibitory synapses in hippocampal dendrites. *Nat. Neurosci.* **7**, 373-379.
Mammoto, A., Sasaki, T., Asakura, T., Hotta, I., Imamura, H., Takahashi, K., Matsuura, Y., Shirao, T. and Takai, Y. (1998). Interactions of drebrin and gephyrin with profilin. *Biochem. Biophys. Res. Commun.* **243**, 86-89.
Matus, A. (2000). Actin-based plasticity in dendritic spines. *Science* **290**, 754-758.
Matus, A., Ackermann, M., Pehling, G., Byers, H. R. and Fujiwara, K. (1982). High actin concentrations in brain dendritic spines and postsynaptic densities. *Proc. Natl. Acad. Sci. USA* **79**, 7590-7594.
McKernan, R. M. and Whiting, P. J. (1996). Which GABAA-receptor subtypes really occur in the brain? *Trends Neurosci.* **19**, 139-143.
Papa, M., Bundman, M. C., Greenberger, V. and Segal, M. (1995). Morphological analysis of dendritic spine development in primary cultures of hippocampal neurons. *J. Neurosci.* **15**, 1-11.
Prange, O., Wong, T. P., Gerrow, K., Wang, Y. T. and El-Husseini, A. (2004). A balance between excitatory and inhibitory synapses is controlled by PSD-95 and neuroligin. *Proc. Natl. Acad. Sci. USA* **101**, 13915-13920.
Rami, G., Caillard, O., Medina, I., Pellegrino, C., Fattoum, A., Ben-Ari, Y. and Ferhat, L. (2006). Change in the shape and density of dendritic spines caused by overexpression of acidic calponin in cultured hippocampal neurons. *Hippocampus* **16**, 183-197.
Richter, K., Langnaese, K., Kreutz, M. R., Olias, G., Zhai, R., Scheich, H., Garner, C. C. and Gundelfinger, E. D. (1999). Presynaptic cytomatrix protein bassoon is localized at both excitatory and inhibitory synapses of rat brain. *J. Comp. Neurol.* **408**, 437-448.
Rothkegel, M., Mayboroda, O., Rohde, M., Wucherpfennig, C., Valenta, R. and Jockusch, B. M. (1996). Plant and animal profilins are functionally equivalent and stabilize microfilaments in living animal cells. *J. Cell Sci.* **109**, 83-90.
Rubenstein, J. L. and Merzenich, M. M. (2003). Model of autism: increased ratio of excitation/inhibition in key neural systems. *Genes Brain Behav.* **2**, 255-267.
Sasaki, Y., Hayashi, K., Shirao, T., Ishikawa, R. and Kohama, K. (1996). Inhibition by drebrin of the actin-bundling activity of brain fascin, a protein localized in filopodia of growth cones. *J. Neurochem.* **66**, 980-988.
Sekino, Y., Kojima, N. and Shirao, T. (2007). Role of actin cytoskeleton in dendritic spine morphogenesis. *Neurochem. Int.* **51**, 92-104.
Shim, K. S. and Lubec, G. (2002). Drebrin, a dendritic spine protein, is manifold decreased in brains of patients with Alzheimer's disease and Down syndrome. *Neurosci. Lett.* **324**, 209-212.
Shirao, T., Hayashi, K., Ishikawa, R., Isa, K., Asada, H., Ikeda, K. and Uyemura, K. (1994). Formation of thick, curving bundles of actin by drebrin A expressed in fibroblasts. *Exp. Cell Res.* **215**, 145-153.
Takahashi, H., Sekino, Y., Tanaka, S., Mizui, T., Kishi, S. and Shirao, T. (2003). Drebrin-dependent actin clustering in dendritic filopodia governs synaptic targeting of postsynaptic density-95 and dendritic spine morphogenesis. *J. Neurosci.* **23**, 6586-6595.
Takahashi, H., Mizui, T. and Shirao, T. (2006). Down-regulation of drebrin A expression suppresses synaptic targeting of NMDA receptors in developing hippocampal neurones. *J. Neurochem.* **97 Suppl. 1**, 110-115.
Turrigiano, G. G. and Nelson, S. B. (2004). Homeostatic plasticity in the developing nervous system. *Nat. Rev Neurosci* **5**, 97-107.
Turrigiano, G. G., Leslie, K. R., Desai, N. S., Rutherford, L. C. and Nelson, S. B. (1998). Activity-dependent scaling of quantal amplitude in neocortical neurons. *Nature* **391**, 892-896.
Yahara, I., Harada, F., Sekita, S., Yoshihira, K. and Natori, S. (1982). Correlation between effects of 24 different cytochalasins on cellular structures and cellular events and those on actin *in vitro*. *J. Cell Biol.* **92**, 69-78.
Yuste, R. and Bonhoeffer, T. (2001). Morphological changes in dendritic spines associated with long-term synaptic plasticity. *Annu. Rev. Neurosci.* **24**, 1071-1089.

Neuroscience 152 (2008) 670–682

EXPRESSION OF DREBRIN E IN MIGRATING NEUROBLASTS IN ADULT RAT BRAIN: COINCIDENCE BETWEEN DREBRIN E DISAPPEARANCE FROM CELL BODY AND CESSATION OF MIGRATION

M. SONG,[a,b] N. KOJIMA,[a] K. HANAMURA,[a] Y. SEKINO,[a,c,d] H. K. INOUE,[e] M. MIKUNI[b] AND T. SHIRAO[a]*

[a]*Department of Neurobiology and Behavior, Gunma University Graduate School of Medicine, 3-39-22 Showa-machi, Maebashi, Gunma 371-8511, Japan*

[b]*Department of Psychiatry and Human Behavior, Gunma University Graduate School of Medicine, Maebashi, Gunma 371-8511, Japan*

[c]*Division of Neuronal Network, Institute of Medical Science, University of Tokyo, Minato-ku, Tokyo, 108-8639, Japan*

[d]*CREST, Japan Science and Technology Agency, Kawaguchi, Saitama 332-0012, Japan*

[e]*Institute of Neural Organization, Fujioka, 375-0021, Japan*

Abstract—Migrating neuroblasts in the adult brain form the rostral migratory stream (RMS) from the lateral ventricle to the olfactory bulb (OB) and then differentiate in the OB. In this study, we immunohistochemically analyzed drebrin expression in the RMS of the adult rat brain. Although drebrin is concentrated in dendritic spines of mature neurons, drebrin-immunopositive (DIP) cell bodies were observed in the RMS. The polysialated form of a neural cell adhesion molecule (PSA-NCAM) was detected in DIP cells. K_i-67, a marker of proliferating cells, was also detected in a subset of DIP cells; however, neither glial fibrillary acidic protein, nestin nor vimentin was detected in DIP cells. These results indicate that DIP cells in the RMS are migrating neuroblasts. An image subtraction method, based on using anti-pan-drebrin and anti-drebrin A antibodies, demonstrated that DIP migrating neuroblasts are immunopositive for drebrin E but not for drebrin A (E+A−). Furthermore, olfactory bulbectomy increased the number of cells with drebrin E+A− signals in the RMS, indicating that these cells migrate along the RMS. Drebrin E+A− cells were also found in the subgranular layer of the dentate gyrus and in the piriform cortex. Thus, detection of drebrin E+A− signals is useful for identifying migrating neuroblasts in the adult brain. In the OB, drebrin E+A− signals were observed in the cell bodies of migrating neuroblasts in the core region; however, only fibrous and punctate drebrin E+A− signals were observed in postmigratory neuroblasts at the outer layers. These data demonstrate that the disappearance of drebrin E+A− signals from the cell body coincides with the cessation of neuronal migration. The disappearance of drebrin E from the cell body may be a molecular switch for the cessation of migration in newly generated neuroblasts.

Key words: actin cytoskeleton, doublecortin, adult neurogenesis, rostral migratory stream, olfactory bulb, piriform cortex.

Neurogenesis continuously occurs in the subventricular zone (SVZ) of the lateral ventricles (LVs) in the adult brain (for review, see Garcia-Verdugo et al., 1998). Newly generated neuroblasts migrate in the rostral migratory stream (RMS) to the olfactory bulb (OB) (Lois and Alvarez-Buylla, 1994). Because many proteins with strong genetic or biochemical links to cytoskeletons are involved in human disorders accompanied by abnormal neuronal migration (for review, see Gleeson and Walsh, 2000), cytoskeletons are believed to play a pivotal role in neuronal migration. The microtubule cytoskeleton is thought to play a role in neuronal migration in the adult and developing brains (Gleeson et al., 1999; Lambert de Rouvroit and Goffinet, 2001). For example, doublecortin (DCX), which binds to microtubules, is expressed in migrating neuroblasts of the adult brain (Francis et al., 1999; Gleeson et al., 1999). Although knockout of just the DCX gene causes only a subtle effect (Corbo et al., 2002; Koizumi et al., 2006), acute knockdown by electroporation of RNAi *in utero* (Bai et al., 2003) and the knockout of both DCX and DCX-like kinase genes (Deuel et al., 2006) result in a severe migration defect in the cerebral cortical neurons. The actin cytoskeleton is also involved in neuronal migration in the developing brain. For example, mutation in filamin 1, a cross-linking protein of actin filaments, prevents the migration of cerebral cortical neurons in human periventricular heterotopia (Fox et al., 1998). However, the expression of filamin 1 in the RMS of the adult brain has not been observed, and is almost restricted to blood vessels and reactive astrocytes (Zhang et al., 1998). Thus, the involvement of the actin cytoskeleton in adult neuronal migration has not yet been clarified.

Drebrin, a side-binding protein of actin filaments that was originally identified in the developing brain (Shirao and Obata, 1985), is involved in cell migration (Shirao et al., 1990; Peitsch et al., 2006). It has two major isoforms, E and A (Shirao et al., 1989), which are generated by alternative splicing from a single gene (Kojima et al., 1993). The amino acid sequences of drebrins E and A are almost

*Corresponding author. Tel: +81-27-220-8052; fax: +81-27-220-8053.
E-mail address: tshirao@med.gunma-u.ac.jp (T. Shirao).

Abbreviations: DAPI, 4′,6-diamidino-2-phenylindole dihydrochloride; DCX, doublecortin; DG, dentate gyrus; DIP, drebrin-immunopositive; DIV, day(s) *in vitro*; GCL, granule cell layer; GFAP, glial fibrillary acidic protein; Ig, immunoglobulin; LV, lateral ventricle; OB, olfactory bulb; OBX, olfactory bulbectomy; PBS, phosphate-buffered saline; PSA-NCAM, polysialated form of neural cell adhesion molecule; RMS, rostral migratory stream; SD, Sprague–Dawley; SDS, sodium dodecyl sulfate; SDS-PAGE, SDS-polyacrylamide gel; SGL, subgranular layer; SVZ, subventricular zone.

0306-4522/08$32.00+0.00 © 2008 IBRO. Published by Elsevier Ltd. All rights reserved.
doi:10.1016/j.neuroscience.2007.10.068

identical except for an internal insert sequence (ins2) in drebrin A. Drebrin E is ubiquitous and predominates in the developing brain (Shirao and Obata, 1986; Shirao et al., 1990; Kojima et al., 1993). In contrast, drebrin A is neuron-specific and predominates in the adult forebrain (Shirao et al., 1989; Kojima et al., 1993). Drebrin is distributed throughout the entire cell body and processes in the developing brain (Shirao and Obata, 1986); however, it is highly concentrated in dendritic spines in the adult brain (Shirao et al., 1987; Hayashi et al., 1996). We previously observed intense drebrin immunostaining by an anti-pan-drebrin antibody in the RMS of the postnatal rat brain (Shirao et al., 1993). Although this suggests that drebrin is involved in adult brain neuronal migration, the isoform of drebrin in the RMS has not been elucidated because of the difficulty in isoform-specific identification. Recently, we have developed a polyclonal antibody that specifically recognizes drebrin A but not drebrin E (Aoki et al., 2005). This antibody will enable us to identify the drebrin isoform in the RMS.

Here, we immunohistochemically investigate the expression of drebrin isoforms in the RMS using anti-pan-drebrin and anti-drebrin A antibodies, and show that migrating neuroblasts possess drebrin E but not drebrin A. Furthermore, we demonstrated that the cessation of neuronal migration in the adult brain coincides with the disappearance of drebrin E from the cell body.

EXPERIMENTAL PROCEDURES

Animals

Eight-week-old male Sprague–Dawley (SD) rats (Charles River Laboratories, Yokohama, Japan) were individually housed in a temperature- and humidity-controlled room in a 12-h light/dark cycle with food and water available *ad libitum*. For cell culture, pregnant Wistar rats (Charles River Laboratories) were used. All animal treatments were performed in accordance with regulations outlined by Japanese law and the NIH guidelines, and were approved by the Animal Care and Experimentation Committee of Gunma University, Showa Campus. Efforts were made to minimize the number of animals used and their pain and discomfort.

Immunohistochemistry

Under pentobarbital anesthesia (50 mg/kg body weight, i.p.; Dainippon-Sumitomo Pharmaceutical, Osaka, Japan), the rats were perfused transcardially with saline containing 2 IU/ml heparin, then with 4% paraformaldehyde in 0.1 M phosphate buffer (pH 7.4). Their brains were removed and postfixed in formaldehyde solution for 1 h at 4 °C. After the brains were immersed in 30% sucrose solution in phosphate-buffered saline (PBS) for at least 24 h, coronal or sagittal sections (10 μm thick) were cut on a cryostat (Leica CM3000, Leica Microsystems, Nussloch, Germany) and mounted onto silane-coated glass slides.

The sections were pretreated with 0.1% Triton X-100 in PBS for 15 min and washed with PBS. After blocking with 3% bovine serum albumin in PBS for 1 h, the sections were incubated with primary antibodies. For K_i-67 staining, the sections were further treated three times in 10 mM citric buffer (pH 6.0) for 5 min each using a microwave processor (750 W; Energy Beam Sciences, Agawam, MA, USA) before the above-described pretreatment.

Two types of antibody raised in our laboratory were used for detecting the drebrin isoforms. The mouse monoclonal antibody M2F6 recognizes both drebrin E and drebrin A isoforms (Shirao and Obata, 1986). The rabbit polyclonal antibody against the partial peptide sequence of a drebrin A-specific insert (FIKASDSGPSSS) (residues 325–336), DAS2, specifically recognizes drebrin A (Aoki et al., 2005).

The sections were incubated with M2F6 (hybridoma supernatant) overnight at 4 °C and washed with PBS. Then, they were incubated with biotinylated anti-mouse immunoglobulin (Ig)G (1:200, Vector Laboratories, Burlingame, CA, USA) for 1 h, washed and incubated with an avidin–biotin–peroxidase complex (Vectastain Elite ABC kit, Vector Laboratories) for 45 min. After washing, immunoreaction was visualized with diaminobenzidine. For the DAS2 staining (1:1000), biotinylated anti-rabbit IgG (1:200, Vector Laboratories) was used as the secondary antibody.

For double immunostaining using a combination of monoclonal and polyclonal antibodies, DAS2 (1:1000), an anti-K_i-67 antibody (1:200, DBS, Pleasanton, CA, USA), an anti-glial fibrillary acidic protein (GFAP) antibody (1:2, Zymed, San Francisco, CA, USA), anti-nestin antibody (1:100, Santa Cruz Biotechnology, Santa Cruz, CA, USA) and anti-vimentin antibody (1:200, Santa Cruz Biotechnology) were each directly diluted in a hybridoma supernatant containing M2F6. The sections were incubated with the primary antibodies for 2 days at 4 °C and washed. Then, they were incubated with a mixture of biotinylated anti-mouse IgG (1:200, Vector Laboratories), rhodamine-conjugated anti-rabbit IgG (1:200, Chemicon, Temecula, CA, USA) and 4′,6-diamidino-2-phenylindole dihydrochloride (DAPI, 1:1000, Molecular Probes, Eugene, OR, USA) for 1 h at room temperature, washed and incubated with fluorescein streptavidin solution (1:100, diluted in PBS, pH 8.2, Vector Laboratories) for 1 h. After washing, the sections were embedded in PermaFluor mounting medium (Thermo Electron, Pittsburgh, PA, USA) and observed under a Zeiss Axioplan 2 microscope system (Zeiss, Jena, Germany).

For the double immunostaining of drebrin and the polysialated form of a neural cell adhesion molecule (PSA-NCAM), a mouse monoclonal antibody 12E3 (IgM, hybridoma supernatant) that specifically recognizes PSA-NCAM (Seki and Arai, 1991) was mixed with M2F6 (1:1 dilution). The sections were incubated with the resulting mixture overnight at 4 °C and washed. Then, they were incubated with a mixture of biotinylated anti-mouse IgG (γ-chain-specific, 1:50, Vector Laboratories) and Texas Red–conjugated anti-mouse IgM (μ-chain-specific, 1:100, Vector Laboratories) for 1 h at room temperature, washed and processed for fluorescein streptavidin labeling as described above.

For triple immunostaining using M2F6, DAS2 and an anti-DCX antibody, the sections were first incubated with a goat anti-DCX antibody (1:100, Santa Cruz Biotechnology) overnight at 4 °C. Then, they were incubated with Cy5-conjugated anti-goat IgG (1:100; Chemicon) as the secondary antibody for 1 h at room temperature. Next, the sections were incubated with a mixture of M2F6 and DAS2 (1:1000) for 2 days at 4 °C. The mixture of the secondary antibodies included biotinylated anti-mouse IgG (1:200), rhodamine-conjugated anti-rabbit IgG (1:100), and DAPI (1:1000). The sections were then incubated with the mixture of the secondary antibodies for 1 h at room temperature and processed for fluorescein streptavidin labeling as described above.

Olfactory bulbectomy (OBX) and cell counting

Eight-week-old male SD rats were anesthetized with pentobarbital (50 mg/kg body weight, i.p.) and fixed in a stereotaxic frame (Narishige, Tokyo, Japan). A skin incision was made on the scalp to expose the skull. A hole of 3 mm diameter was drilled above the right OB. Then, the right OB was exposed and removed by aspiration with a needle connected to a water pump. Caution was taken to avoid damaging the contralateral unoperated side. The cavity was packed with sterilized Gelform (Pfizer, Tokyo, Japan), and the skin was sutured. The animals were placed in a warm cage to maintain their body temperature until they recovered from the anesthesia. Then, they were returned to their home cages. Transcardial perfusion was performed 1 week after the surgery.

Immunohistochemical analysis was carried out as described above using coronal sections that included the RMS.

Because no RMS cells were immunostained with DAS2, we used M2F6 immunostaining for cell counting after OBX. Two sections approximately 4.2 mm and 4.7 mm apart from the bregma in the rostral direction (Paxinos and Watson, 1998) of each animal were immunostained, and contiguous images of each section were acquired using a 63× oil immersion objective lens so that they cover the whole area of the RMS in each section. Montages were made from the images using Adobe Photoshop 7.0 software (Adobe Systems, San Jose, CA, USA). The cells on each side of the two sections were counted. Then, the average number of cells of each animal was calculated and presented as mean±S.E.M. A two-tailed paired Student's *t*-test was performed to determine the statistical significance of difference in the number of cells between the operated and unoperated sides.

Sample preparation and Western blotting

After deep anesthesia, brains were quickly removed from rat. After isolating the OB, the remaining part of the brain was immediately frozen by dry ice. For the SVZ, coronal sections (150 μm thick) were cut on a cryostat, and the brain region containing the SVZ was dissected out under a binocular microscope. The dissected tissue was homogenized in a minimal amount of sodium dodecyl sulfate (SDS) sample buffer and boiled for 5 min. Protein sample was electrophoretically separated on 8% SDS-polyacrylamide gel (SDS-PAGE), transferred onto a polyvinylidene difluoride transfer membrane (Immobilon-P; Millipore, Billerica, MA, USA), and probed with an anti-pan-drebrin (M2F6) or an anti-drebrin A (DAS2) antibody. Following incubation with the horseradish peroxidase–conjugated second antibody, immunoreactive signals were visualized on X-ray film (Hyperfilm-ECL; GE Healthcare, Piscataway, NJ, USA) by ECL detection reagents (GE Healthcare).

Image subtraction for identifying signal of drebrin E without drebrin A

We used an image subtraction using two anti-drebrin antibodies, M2F6 and DAS2, to identify the signal for drebrin E but not for drebrin A (E+A−) from total drebrin signals. Since a drebrin E-specific antibody is not available, we used anti-pan-drebrin antibody instead of drebrin E-specific antibody in the subtraction methods. Images of M2F6 and DAS2 staining were separately acquired using a Zeiss Axioplan 2 microscope system (Zeiss) equipped with a cooled charge-coupled device camera (CoolSnap fx, Photometrics, Tucson, AZ, USA). The exposure time for each image was adjusted using MetaMorph software (Molecular Devices, Sunnyvale, CA, USA), so that the intensities of the neuropils matched each other. Using the image arithmetic function in MetaMorph, we subtracted the image of DAS2 from that of M2F6 to visualize E+A− signals.

Fig. 1 shows that this image subtraction enables the discrimination of 0-day-*in vitro* (DIV) neurons from 21-DIV neurons. Primary hippocampal cultures were prepared as previously de-

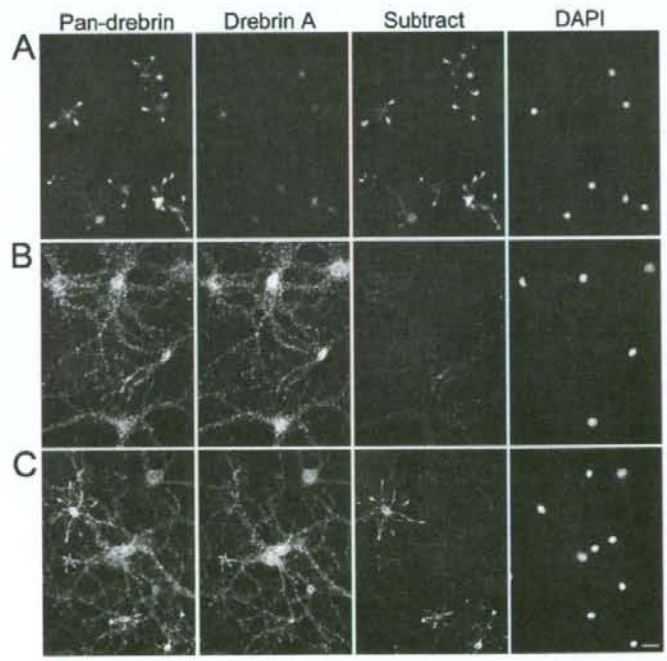

Fig. 1. Identification of drebrin E+A− signals *in vitro* by image subtraction. (A) 0-DIV neurons. (B) 21-DIV neurons. (C) 0-DIV neurons inoculated onto 21-DIV neurons. The left and middle-left panels show images of neurons immunostained with anti-pan-drebrin (M2F6) and anti-drebrin A (DAS2) antibodies, respectively. The middle-right panels show the subtraction images obtained by subtracting the middle-left images from the left panel images. The right panels show DAPI immunostaining images. M2F6 immunostained both 0-DIV and 21-DIV neurons (left panels). DAS2 immunostained only 21-DIV neurons (middle-left panels). The subtraction images showed that only aspiny neurons with short neurites have drebrin E+A− signals (middle-right panels of A and C). Note that the subtraction images of 21-DIV neurons showed no cell with E+A− signals (middle-right panels of B). Scale bar=20 μm.

scribed (Takahashi et al., 2003). Double-immunofluorescence staining was performed as described above. Zero-DIV neurons were immunostained with M2F6 but not with DAS2, and were identified as cells with drebrin E+A− signals by the image subtraction (Fig. 1A). On the other hand, 21-DIV neurons were immunostained with both M2F6 and DAS2, and were not identified as drebrin E+A− cells (Fig. 1B). This is consistent with the results of previous studies that showed the presence of drebrins E and A in 21-DIV neurons by immunoblotting (Takahashi et al., 2006). In a mixed culture of 0-DIV and 21-DIV neurons, a larger number of neurons were detected in M2F6 images than in DAS2 images (Fig. 1C). The subtraction images showed only aspiny neurons with short neurites as drebrin E+A− cells, which has a characteristic of 0-DIV neurons. Thus, this subtraction method using anti-pan-drebrin and anti-drebrin A antibodies is useful for identifying cells possessing only drebrin E but not drebrin A.

RESULTS

Intense drebrin immunostaining in RMS of adult rat brain

Immunohistochemical analysis using the anti-pan-drebrin antibody M2F6 demonstrated an intensely immunostained stream along the route of the SVZ and RMS (arrows in Fig. 2A, C), through which newly generated neuroblasts migrate to the OB. This intensely stained drebrin-immunopositive (DIP) stream spread in the OB (Fig. 2E). In contrast to M2F6, the drebrin A-specific antibody DAS2 did not immunostain the stream (Fig. 2B, D, F); however, both DAS2 and M2F6 similarly stained the neuropil regions of the adult cerebral cortex (CX in Fig. 2A, B). Therefore, the absence of a stream immunostained by DAS2 in the SVZ-RMS suggests the differential distribution of the drebrin isoforms in this region.

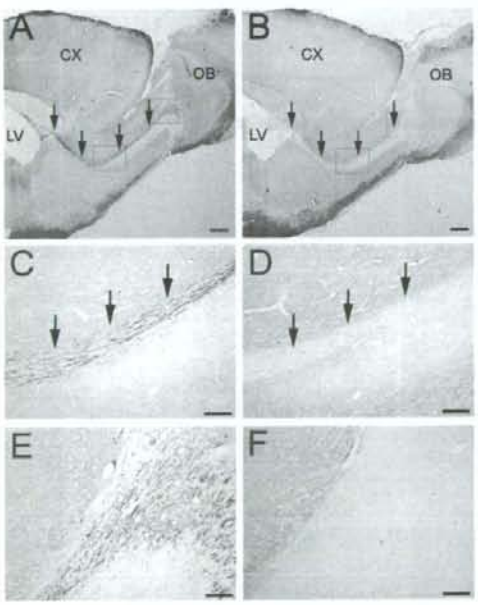

Fig. 2. Immunostaining of drebrin of adult rat forebrain. Sagittal sections of the forebrain were immunostained with M2F6 (A, C and E) and DAS2 (B, D and F). Intense immunostaining along the route of the SVZ and RMS (indicated by arrows) was observed from the LV to the OB in A, but not in B. C and D show magnified images of the lower-left red boxes in A and B, respectively. E and F show magnified images of the upper-right red boxes in A and B, respectively. Note that the stream spreads in the OB (E). CX, cerebral cortex. Scale bars = 500 μm A, B; C–F, 100 μm.

Immunocytochemical characterization of DIP cells in SVZ-RMS

Immunofluorescence microscopy at a higher magnification revealed that intense drebrin immunostaining was observed in the cell bodies in the SVZ-RMS (left panels in Fig. 3). To further characterize these DIP cells, we carried out double-immunofluorescence staining with various types of cell marker.

K_i-67 is a marker of dividing cells expressed during all cell cycle phases except G_0, and is often used for labeling proliferating cells in adult neurogenic regions (Scholzen and Gerdes, 2000; Kee et al., 2002). In the SVZ-RMS, K_i-67 immunostaining within the nuclei was observed in a subset of DIP cell nuclei (Fig. 3A, B), although the population of double-immunostained cells varied in the longitudinal axis (Supplemental Fig. 1). The result indicates that a subset of the DIP cells in the RMS was in the stage of cell division or immediately after cell division.

PSA-NCAM is expressed in newly generated neurons in the SVZ-RMS (Doetsch and Alvarez-Buylla, 1996; Doetsch et al., 1997). The double-immunostaining of drebrin and PSA-NCAM showed that most of the DIP cells possessed PSA-NCAM in their cell bodies in the SVZ-RMS (Fig. 3C, D).

GFAP is a marker of astrocytes and stem cells in the adult SVZ (Doetsch et al., 1999). In the SVZ-RMS, DIP cell bodies were frequently observed adjacent to or surrounded by GFAP-immunopositive cells; however, they did not overlap with each other (Fig. 3E, F), indicating that neither astrocytes nor stem cells have DIP cell bodies. Moreover, the DIP cell bodies surrounded by the GFAP-immunopositive cells showed similar spatial relationships between migrating neuroblasts and glial tubes reported in the SVZ-RMS (Lois et al., 1996; Peretto et al., 1997).

Nestin and vimentin are intermediate filament proteins, and they are used as markers of astrocytes and ependymal cells in the adult SVZ (Doetsch et al., 1997). As shown in Fig. 4, the cells in the ependymal layer of the SVZ were intensely stained by anti-nestin and anti-vimentin antibodies, but were not stained by the anti-drebrin antibody.

Drebrin E+A− signals of DIP cells in SVZ-RMS

By the subtraction of the DAS2 images from the M2F6 images, drebrin E+A− signals were highlighted. All the DIP cell bodies in the SVZ-RMS had E+A− signals (Fig. 5). They largely accumulated in the dorsolateral region of the LV and in the RMS (Fig. 5A, B, C). We observed a larger number of DIP cell bodies in the anterior SVZ than in the posterior SVZ (data not shown). Cells with E+A− signals formed a nest-like

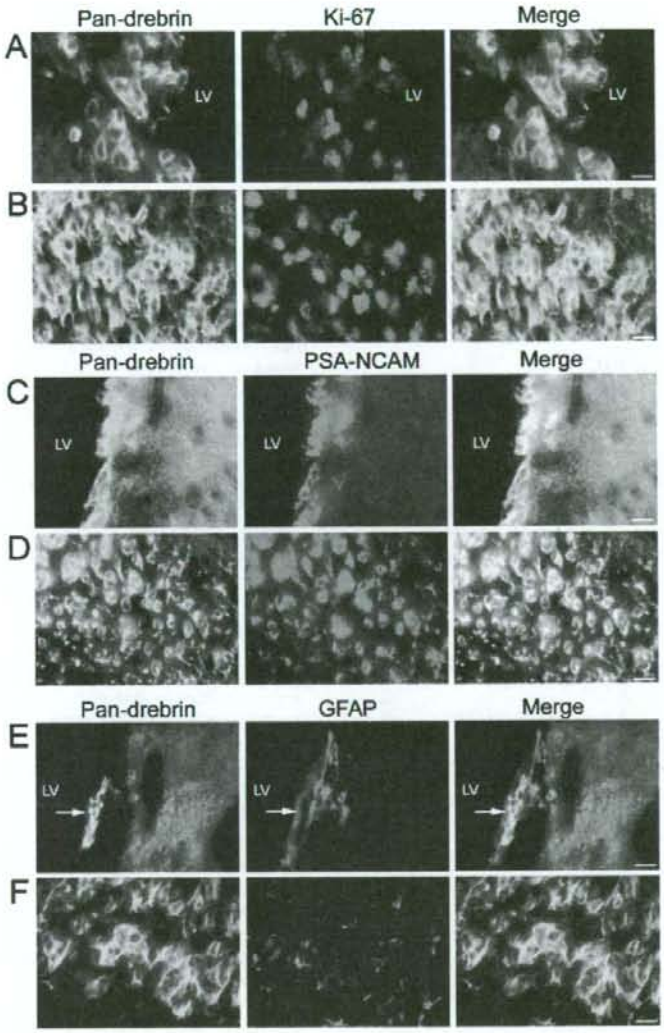

Fig. 3. Double-immunofluorescence staining of drebrin with K_i-67, PSA-NCAM and GFAP in the SVZ and RMS. A, C and E show images of the SVZ, and B, D and F show those of the RMS. Sets of A and B, C and D, and E and F were double-immunostained using M2F6 (left panels, green) with anti-K_i-67, anti-PSA-NCAM and anti-GFAP antibodies (middle panels, red), respectively. The right panels show merged images of the left and middle panels. A large number of DIP cells have K_i-67-positive nuclei (A, B). All DIP cells are PSA-NCAM-immunopositive (C, D). There is no overlap of drebrin and GFAP immunostainings (E, F). Note that DIP cell clusters are surrounded by GFAP-immunopositive cells (arrows in E). Scale bars=10 μm.

structure in the SVZ of the LV and in the RMS (in Fig. 5B, D). In the sagittal section, cells with drebrin E+A− signals formed a chain-like structure in the RMS directed toward the OB, and showed monopolar and bipolar shapes (right panel in Fig. 5D). Their elongated cell bodies were small with a diameter of 2.78±0.62 μm (n=130). The morphological characteristics described here are consistent with those of migrating neuroblasts reported previously (Doetsch and Alvarez-Buylla, 1996; Doetsch et al., 1997; Peretto et al., 1999).

Increase in number of DIP cells in RMS after OBX

OBX results in an increase in RMS volume on the operated side without a change in RMS cell-packing density, because neuroblasts in the RMS continuously migrate and accumulate in the rostral region near the excision site (Kirschenbaum et al., 1999). Therefore, to confirm whether DIP cells in the RMS continuously migrate, we unilaterally removed the OB. One week after the surgery, the area of

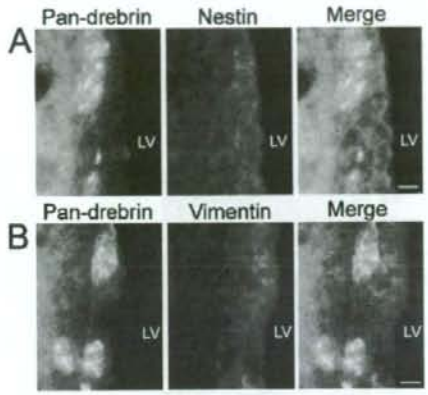

Fig. 4. Double-immunofluorescence staining of drebrin with nestin and vimentin in SVZ. The images are immunostained using M2F6 (left panels, green), anti-nestin antibody (middle panel in A, red) and anti-vimentin antibody (middle panel in B, red). The right panels show merged images from the left and middle panels. The ependymal cells are intensely immunostained by anti-nestin and anti-vimentin antibodies. There is no overlap of drebrin immunostaining with immunostaining for either nestin or vimentin. Scale bars=10 μm.

drebrin E+A− signals on the operated side enlarged relative to that on the unoperated side (Fig. 6A). Quantitative analysis revealed that the number of DIP cell bodies on the operated side (803±91 cells, n=4) was significantly larger than that on the unoperated side (549±47 cells, n=4, P<0.05) (Fig. 6B). This indicates that OBX results in an increase in the number of DIP cells.

Disappearance of drebrin E+A− signals in outer layers of OB

Drebrin E+A− signals were observed not only in the SVZ-RMS, but also in the OB where neurons stop migrating (Fig. 7). Drebrin E+A− cells were clustered in the core of the OB (Fig. 7B), but scattered in the granule cell layer (GCL; Fig. 7C). They had bipolar cell shapes with prominent processes in the radial direction in the GCL (arrow in Fig. 7C). In the outer layers of the OB, the number of cell bodies with drebrin E+A− signals decreased markedly. In the plexiform and glomerular layers, drebrin E+A− signals were hardly observed except for a few fibrous and dot-like staining patterns (Fig. 7D, E).

Western blotting analysis of drebrin isoforms in SVZ-RMS and OB

We next biochemically identified the drebrin isoforms expressed in the SVZ and OB. As shown in Fig. 8, Western blotting using the anti-pan-drebrin antibody recognized two immunopositive bands in the extracted proteins from the tissue containing the SVZ or OB of adult rats. No other immunopositive bands were detected. Upper and lower bands corresponded to drebrin A and drebrin E, respectively by their migration pattern on SDS-PAGE (Shirao et al., 1989). Furthermore, the anti-drebrin A antibody DAS2 specifically recognized the upper band. These biochemical data showed that drebrin E was expressed in the SVZ-RMS and OB of adult rats. Although drebrin E content was relatively weak in the tissue containing the SVZ, it might be due to the contamination of the surrounding regions, such as striatum that contains a high level of drebrin A.

Comparison of distribution pattern between drebrin and DCX in SVZ-RMS-OB system

Because DCX is expressed in newly generated neurons of the adult brain (Nacher et al., 2001; Brown et al., 2003), we carried out triple immunostaining to compare the distribution patterns of drebrin and DCX. In the SVZ-RMS, drebrin E+A− cells were immunostained with an anti-DCX antibody (Fig. 9A, B). In the GCL of the OB, on the other hand, only a small population of DCX-immunopositive cells, which showed a bipolar shape, had drebrin E+A− signals (arrow in Fig. 9C). Most DCX-immunopositive cells hardly had drebrin E+A− signals in their cell bodies, although a few fibrous and dot-like patterns of drebrin E+A− signals were observed. These DCX-immunopositive cells without drebrin E+A− signals showed a mature morphology with apical dendrites extending to the plexiform layer (Fig. 9D). On the other hand, DIP signals revealed by immunostaining with M2F6 and DAS2 antibodies showed dot-like staining patterns similar to those observed in neuropil regions in the adult brain (Supplemental Fig. 2).

DIP cells in dentate gyrus (DG) of hippocampus

The DG of the hippocampus is another neurogenic region in the adult rat brain. Some cells clustered in the subgranular layer (SGL) were strongly immunostained with M2F6 (left panel in Fig. 10A). These clustered DIP cells had drebrin E+A− signals and had smaller cell bodies than the granule cells (Fig. 10A). They were GFAP-immunonegative (Fig. 10B) and most of them were K_i-67-immunopositive (Fig. 10C), similarly to the DIP cells in the SVZ-RMS.

We then examined the relationship between the distributions of drebrin E+A− signal and DCX. Some DCX-immunopositive neurons in the SGL had drebrin E+A− signals (Fig. 11A). In contrast, DCX-immunopositive cells in the granular layer, which showed a mature morphology with apical dendrites, had no drebrin E+A− signals (Fig. 11B).

Cells with drebrin E+A− signals in piriform cortex

We examined whether drebrin E+A− cells are present in the adult piriform cortex, where PSA-NCAM-immunopositive (Seki and Arai, 1991) and DCX-immunopositive cells (Nacher et al., 2001) have been reported. The subtracted images demonstrated that drebrin E+A− cells are distributed sporadically, but that they sometimes form clusters in layer II (densely packed small pyramidal cell layer) of the piriform cortex. DCX was localized in all of these drebrin E+A− cells (Fig. 12B). On the other hand, DCX-immunopositive cells that have no drebrin E+A− signals were also observed in layer II (arrows in Fig. 12C). They extended their apical dendrites to layer I (cell-sparse external

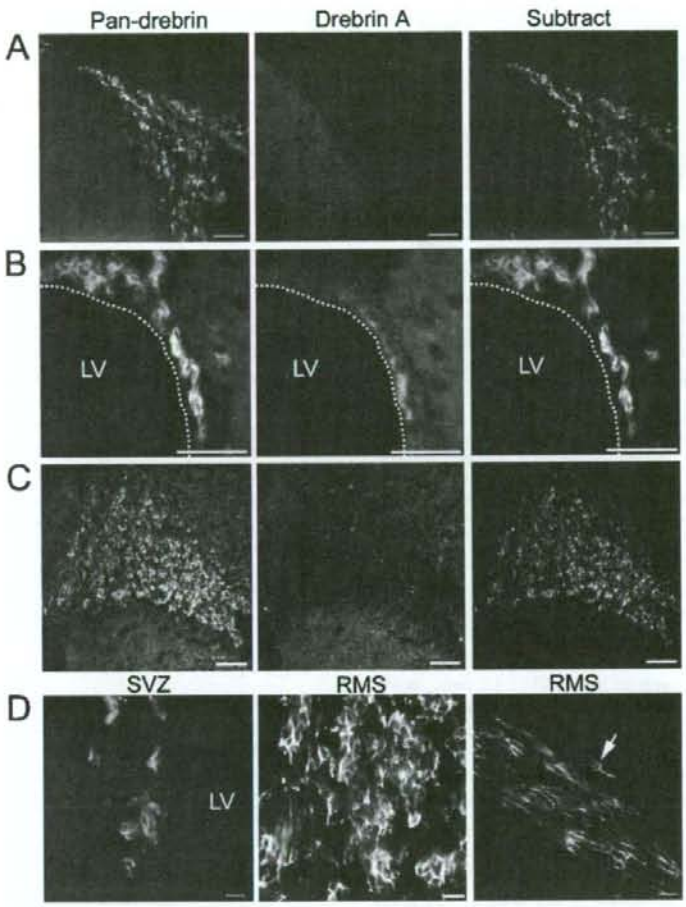

Fig. 5. Double-immunofluorescence staining with two anti-drebrin antibodies in SVZ and RMS of adult rat brain. (A–C) The left and middle panels show images immunostained with anti-pan-drebrin (M2F6) and anti-drebrin A (DAS2) antibodies, respectively. The right panels show the subtraction images obtained by subtracting the middle panel images from the left panel images, showing drebrin E+A− signals. Note that all the cell bodies immunostained with M2F6 have E+A− signals, which accumulated in the dorsolateral region of the SVZ (A, B) and in the RMS (C). The dotted lines in B are the borders of the LV. (D) Higher-magnification images of the subtracted images in the SVZ (left panel), RMS (coronal; middle panel) and RMS (sagittal; right panel). Note that the drebrin E+A− cells are clustered in the coronal images, forming chain-like structures in the sagittal images. Note that some cells have drebrin E+A− signals in their leading processes (arrow) and cell bodies. Scale bars=50 μm, A–C; D, 10 μm.

plexiform layer; Fig. 12), which is a characteristic of mature neurons.

DISCUSSION

In this study, we demonstrate that migrating neuroblasts in the adult SVZ-RMS-OB system have drebrin E+A− signals in their cell bodies. DCX is also expressed in the cell body in the migrating neuroblasts; however, DCX remains to be expressed through migratory and postmigratory stages in adult neurogenesis. Also note that the disappearance of drebrin E+A− signals from the cell body coincides with the cessation of neuronal migration. These results indicate that drebrin E+A− signal is a good marker of migrating neurons in the adult brain, and drebrin E may play an important role in neuronal migration.

DIP cells in adult SVZ-RMS are migrating neuroblasts

DIP cells in the adult SVZ-RMS have small cell bodies and a bipolar shape, which are characteristics of migrating neurons. PSA-NCAM and DCX, which are detected in migrating neuroblasts (Rousselot et al., 1995; Nacher et al., 2001), are also detected in DIP cells. K_i-67 immunostaining shows that some DIP cells are proliferating cells. These results indicate that DIP cells in the SVZ-RMS are migrating neuroblasts. All these DIP cells have drebrin

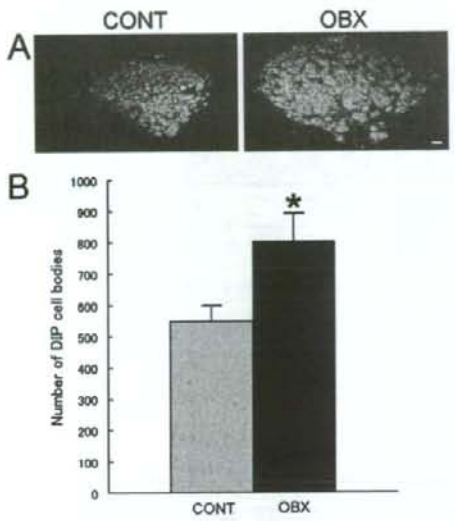

Fig. 6. Effect of OBX on DIP cells in RMS. (A) The subtraction image represents the distribution of drebrin E+A− cells in the unoperated (CONT) and operated (OBX) sides. Note that the area with E+A− signals is larger in the operated side than in the unoperated side. (B) The number of DIP cell bodies in the RMS is significantly increased in the operated side as compared with the unoperated side (n=4; * P<0.05; paired Student's t-test). Data are presented as mean±S.E.M. Scale bar=20 μm.

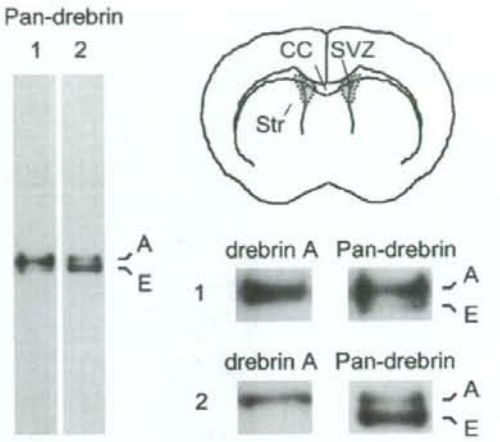

Fig. 8. Immunoblotting of SVZ and OB with two anti-drebrin antibodies. The left panel shows immunoblotting of protein lysate prepared from the tissue including the SVZ (lane 1) and the OB (lane 2) with an anti-pan-drebrin antibody, M2F6. The SVZ tissue dissected out are indicated as shaded areas in the schematic drawing at the upper right side. CC, corpus callosum; Str, striatum. M2F6 reacts with two protein bands corresponding to drebrins E and A in the two protein samples containing the migratory neurons. Note that no protein bands other than these two drebrins were detected. The lower-right panels show immunoblotting of protein samples including the SVZ (1) and the OB (2) with an anti-drebrin A (DAS2) and anti-pan-drebrin (M2F6) antibodies. DAS2 reacts only with the upper band of the M2F6-immunopositive bands.

E+A− signals in their cell bodies, showing that they express only drebrin E but not drebrin A similarly to immature neurons in the developing brain.

Furthermore, OBX increases the number of DIP cells that have E+A− signals on the operated side. This indicates that DIP cells accumulate in a cul-de-sac of the RMS because they continuously migrate rostrally even in the absence of the OB, which is also a characteristic of adult

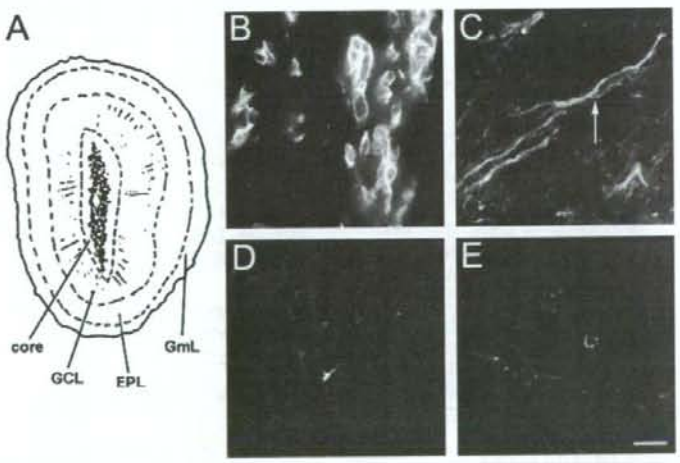

Fig. 7. Drebrin E+A− signals in OB. (A) The schematic drawing shows typical distribution of DIP cells in the OB. (B–E) Subtraction images obtained by subtracting the DAS2 images from the M2F6 images, representing drebrin E+A− signals. (B) Core of OB. Note that cells with drebrin E+A− signals are clustered in the core. (C) GCL. The arrow indicates a bipolar cell with E+A− signals. (D) External plexiform layer (EPL). (E) Glomerular layer (GmL). A few processes are highlighted in EPL and GmL. Note that fibrous and dot-like staining pattern of E+A− signals are occasionally observed. Scale bar=10 μm.

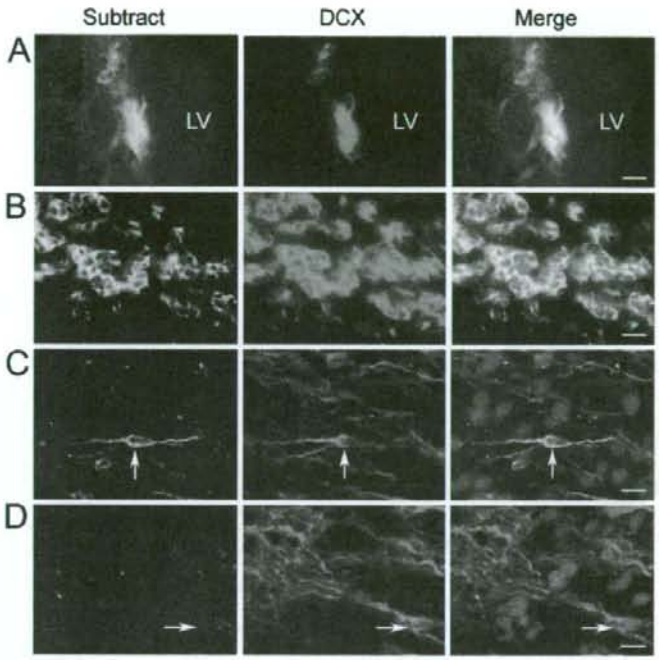

Fig. 9. Comparison of distribution of drebrin E+A− and DCX signals in SVZ and RMS. The left panels show subtraction images obtained by subtracted the DAS2 images from the M2F6 images, representing drebrin E+A− signals. The middle panels show the images of cells immunostained with anti-DCX antibody. The right panels show the merged images of a drebrin E+A− signal (green), a DCX signal (red) and a signal of DAPI, a nuclear marker (blue). (A, B) The images of the SVZ of the LV and RMS, respectively. The colocalization of drebrin E+A− and DCX signals are observed around cell nuclei stained with DAPI in the SVZ and RMS. (C, D) The images of the GCL of the OB. Neurons with apical dendrites were highlighted by DCX signals in the GCL. Note that the colocalization of drebrin E+A− and DCX signals is sometimes observed in bipolar migrating cells (arrows in C). Scale bar=10 μm.

migrating neuroblasts in the SVZ-RMS (Kirschenbaum et al., 1999).

Drebrin E is also expressed in non-neuronal cells outside the brain (Shirao and Obata, 1986; Kojima et al., 1993; Shirao et al., 1994; Peitsch et al., 1999). Furthermore, even non-neuronal cells in the brain may express drebrin E *in vivo*, because astrocytes have drebrin E *in vitro* (Butkevich et al., 2004). This raises the possibility that some of the DIP cells in the SVZ-RMS of the adult brain were non-neuronal cells, such as ependymal cells, stem cells and astrocytes. It has been reported that all ependymal cells, stem cells and astrocytes in the SVZ-RMS express GFAP, nestin and vimentin (Doetsch et al., 1997); however, the examined DIP cells in the adult brain do not have any GFAP, nestin or vimentin immunoreactivity. These data indicate that DIP cells in the RMS are neither ependymal cells, stem cells, nor astrocytes. Taken altogether, DIP cells in the RMS are thought to be migrating neuroblasts.

Migrating neurons in adult piriform cortex

It has been suggested that the reorganization of the neuronal network, involving adult neurogenesis, occurs in the piriform cortex (Seki and Arai, 1991; Peretto et al., 1999). An immunohistochemical study using an anti-DCX antibody showed three types of DCX-immunopositive cell in the adult piriform cortex: clustered small neurons with round cell bodies, medium-sized neurons with globular cell bodies from which two or three apical dendritic trunks emerged, and small cells with a single straight process resembling migratory neuroblasts (Nacher et al., 2001). We showed that DCX-immunopositive neurons with drebrin E+A− signals in the adult piriform cortex have morphological characteristics similar to those of migratory neuroblasts. This strongly indicates the presence of migrating neuroblasts in the adult piriform cortex.

Involvement of change in characteristic of actin cytoskeleton of cell body in cessation of neuronal migration

This study reveals that DIP cells in the SVZ-RMS have E+A− signals in their cell bodies, suggesting that migrating neuroblasts express drebrin E but not drebrin A. However, drebrin E+A− signals disappear in the outer layer of the OB, where neuroblasts stop their migration and start their differentiation. Instead, dot-like patterns of DIP signals, similar to those in the cerebral cortex (Aoki et al., 2005), are observed in the outer layer of the OB, suggest-